Radiation-Induced Brain Structural and Functional Abnormalities in Presymptomatic Phase and Outcome Prediction

Zhongxiang Ding,[1,2] Han Zhang ,[2] Xiao-Fei Lv ,[3] Fei Xie,[3] Lizhi Liu,[3] Shijun Qiu,[4] Li Li,[3]* and Dinggang Shen[2,5]*

[1]*Zhejiang Provincial People's Hospital, Hangzhou, Zhejiang 310014, China*
[2]*Department of Radiology and BRIC, University of North Carolina at Chapel Hill, Chapel Hill, North Carolina, USA*
[3]*Department of Medical Imaging, Collaborative Innovation Center for Cancer Medicine, State Key Laboratory of Oncology in South China, Sun Yat-sen University Cancer Center, Guangzhou 510060, China*
[4]*Medical Imaging Center, The First Affiliated Hospital of Guangzhou University of Chinese Medicine, Guangzhou 510405, China*
[5]*Department of Brain and Cognitive Engineering, Korea University, Seoul 02841, Republic of Korea*

◆━━━━━━━━━━━━━━━━━━━━━━━━━━━━━◆

Abstract: Radiation therapy, a major method of treatment for brain cancer, may cause severe brain injuries after many years. We used a rare and unique cohort of nasopharyngeal carcinoma patients with normal-appearing brains to study possible early irradiation injury in its presymptomatic phase before severe, irreversible necrosis happens. The aim is to detect any structural or functional imaging biomarker that is sensitive to early irradiation injury, and to understand the recovery and progression of irradiation injury that can shed light on outcome prediction for early clinical intervention. We found an acute increase in local brain activity that is followed by extensive reductions in such activity in the temporal lobe and significant loss of functional connectivity in a distributed, large-scale, high-level cognitive function-related brain network. Intriguingly, these radiosensitive functional alterations were found to be fully or partially recoverable. In contrast, progressive late disruptions to the integrity of the related far-end white matter structure began to be significant after one year. Importantly, early increased local brain functional activity was predictive of severe later

temporal lobe necrosis. Based on these findings, we proposed a dynamic, multifactorial model for radiation injury and another preventive model for timely clinical intervention. *Hum Brain Mapp 39:407–427, 2018.* © 2017 *Wiley Periodicals, Inc.*

Key words: radiation therapy; irradiation injury; functional connectivity; structural connectivity; diffusion tensor imaging; functional magnetic resonance imaging; resting state; prognosis; amplitude of low-frequency fluctuations; nasopharyngeal carcinoma

---

INTRODUCTION

Radiation therapy (RT) is a longstanding and routine clinical treatment for cancer. During cranial RT, normal brain tissue along the RT pathway and in proximity to tumors is inevitably irradiated, causing not only transient and reversible abnormalities but also progressive and irreversible late toxicities such as brain tissue necrosis [Acker et al., 1998; Bowen et al., 1996; Chan et al., 2009b; Haddy et al., 2011; Lo et al., 1992; New, 2001]. RT-induced mild cognitive impairment and/or neuropsychiatric disorders also significantly decrease the quality of life [Greene-Schloesser and Robbins, 2012; Khong et al., 2006; Tang et al., 2012; Warrington et al., 2013]. Despite carefully designed irradiation delivery, RT may still result in such sequelae; but our understanding of the large-scale neuromechanism of the post-RT brain injury is still insufficient [Wang et al., 2010; Wong and Van der Kogel, 2004]. An early, *presymptomatic detection* of the post-RT brain injury at the time when no magnetic resonance (MR)-visible lesions have developed is of great importance for early prevention and mitigation of these complications [Gondi et al., 2010].

Investigation of the brain injury in different stages after completion of RT is quite interesting to the neuroscience community, because of the complex time-evolving interplay between brain recovery, plasticity, and degeneration. However, previous studies on brain tumor patients have two major constraints. First, short survival time of brain tumor patients limits the follow-up time for the investigation of *late* irradiation-induced brain abnormalities [Chapman et al., 2012; Nagesh et al., 2008]. Second, the residual brain lesions or recurrences that may not be easily differentiated from the RT-induced injuries [Chan et al., 1999]. In contrast, nasopharyngeal carcinoma patients constitute an ideal cohort for such a study. Nasopharyngeal carcinoma is a malignant tumor originating in the nasopharynx [Chang and Adami, 2006]; RT is a routine clinical treatment [Brennan, 2006] and may inevitably result in irradiation of the normal brain tissue [Chen et al., 2011]. More than 80% of the RT patients survive for five years or longer [Zhou et al., 2013]; long enough for the study of the late effects of RT. However, almost all studies using nasopharyngeal carcinoma patients have focused on *MR-visible* brain injury at the *specific* brain regions (e.g., temporal lobe necrosis), which usually appears many years after RT [Chan et al., 2003; Chen et al., 2011; Chong et al., 2000; Su et al., 2012, 2013; Tang et al., 2014; Tsai et al., 2014; Ye et al., 2012; Zeng et al., 2015; Zheng et al., 2015; Zhou et al., 2013, 2014] at the stage when brain damage has already been *irreversible*. Therefore, the recovery ability is quite limited, and the reverse of the impaired cognitive function is usually impossible [Cheung et al., 2003].

We recently began to investigate RT-induced brain injury in nasopharyngeal carcinoma patients at its *presymptomatic* stage, at which time the patients still have normal-appearing MR or CT images [Wang et al., 2012; Xiong et al., 2013]. These studies, together with only a few other presymptomatic studies on brain tumor patients [Chapman et al., 2012; Matulewicz et al., 2006; Nagesh et al., 2008], focused only on the structural or morphometric changes in the brain white matter. However, these results have largely been inconsistent and have lacked spatial specificity due to the region of interest (ROI)-based analysis strategy. In addition, for these brain tumor studies, inhomogeneous cohorts with different tumor location, pathology and size resulted in different irradiated areas, while the craniotomy and tumor recurrence could have introduced additional confounding effect. However, the most significant issue for these studies is that different predefined ROI placements introduced tremendous variation in the measuring results and led to such inconsistent conclusions. For example, Xiong et al. [2013] calculated diffusion tensor imaging (DTI) metrics in a few preset ROIs within the temporal lobe. They found that the temporal lobe white matter was affected immediately after RT but recovered one year later. However, in another study, fractional anisotropy (FA) values were found to remain abnormally low after one year [Wang et al., 2012]. In a more recent study, Chen et al. [2015] found an acute decrease in FA within 3 months after RT in the anterior temporal lobe, but no data were available for the study of late responses. The above findings, however, were not consistent with those from the brain tumor studies, in which different white matter areas, such as the parahippocampal cingulum bundles [Chapman et al., 2012] and the genu and splenium of the corpus callosum [Nagesh et al., 2008] were assessed and revealed a gradual course towards abnormality, which again indicates progression of structural abnormalities. In addition to DTI, both our group [Wang et al., 2012; Xiong et al., 2013] and another group [Chen et al., 2014] have used magnetic resonance spectroscopy

(MRS) to measure brain tissue metabolism and neuronal function in post-RT, normal-appearing nasopharyngeal carcinoma patients, but this modality is hampered by heavy noise and poor spatial resolution [Jansen et al., 2006], as well as the same ROI-definition problem. More advanced brain functional study using functional magnetic resonance imaging (fMRI) has been largely neglected. Collectively, due to the use of these oversimplified, less detailed, and potentially biased methods of analysis, precise localization of RT-induced brain structural and functional changes in the presymptomatic stage remain largely unknown. A *whole-brain*, *voxel-wise* exploration is highly desirable [Lv et al., 2014] to provide a better understanding of how the brain evolves in the natural post-RT course, during which recovery and progression can dynamically interact.

The aim of this study is to explore RT-induced brain functional abnormality in the *presymptomatic* stage in a voxel-wise manner by taking advantage of relatively high spatial and temporal resolution of fMRI. An additional aim is to try to understand the relationship between functional and structural abnormalities in a long post-RT period, with which we can better characterize the structurally and functionally evolutional processes of the human brain after the completion of RT. It is more clinically important to investigate presymptomatic stage than symptomatic or clinical stage because early alterations, especially those that can be detected by more sensitive imaging and analysis techniques, can potentially be used in the future to predict the outcomes many years later, thereby allowing adequate time for neuroprotective or other preventive treatment. In this article, we report our initial finding based on a prospective, follow-up, pseudo-longitudinal cohort study. To this end, we divided different normal-appearing nasopharyngeal carcinoma patients into four groups: a baseline group (prior to RT, G1) and three post-RT groups (G2, G3, and G4). The patients in the latter three groups were scanned during different post-RT periods ranging from the acute to the delayed response stage (0–6, 6–12, and >12 months for G2, G3, and G4, respectively). For each group, multimodal brain imaging, including rs-fMRI and DTI were conducted for probing both brain function and structure. These patients were similarly treated with RT, regularly followed up with clinical MRI, until some of them showed MRI-visible RT-induced injuries (e.g., temporal lobe necrosis), based on which our detected early imaging biomarker were validated.

Specifically, the brain function was measured by resting-state fMRI (rs-fMRI) using both localized brain activity and inter-regional co-activity (functional connectivity, or FC) as a natural resting state is helpful for detecting aberrance in inherent brain spontaneous activities and their inter-regional coactivity. Based on previous RT-induced focal lesion studies, we believed that, the brain spontaneous activity at the region nearby or in the path of the irradiation (i.e., the *near-end* brain regions) could show early abnormalities. Previous clinical studies have shown that

fractional amplitude of low-frequency fluctuation (fALFF) [Zang et al., 2007; Zou et al., 2008] is a reliable and sensitive metric for such purpose. Therefore, we used fALFF to detect RT-induced local brain functional abnormalities. We also investigated the possible reason of the RT-induced mild cognitive impairment, a common side effect of RT [Greene-Schloesser and Robbins, 2012], using FC based on temporally synchronized brain spontaneous activities because the previous studies have shown that FC or resting-state brain functional network is one of the important neuromechanisms for retaining healthy and normal cognitive functions and responsible for abnormal cognitive abilities or mental disorders [Buckner, 2013]. According to the literature, it is the default mode network (DMN) that has often been found to be mostly related to the mild cognitive impairment due to Alzheimer's disease (AD), Parkinson's disease (PD) and other diseases (e.g., Type-II diabetes), we thus also focused on the FC in the DMN and hypothesized that *both* near- *and* far-end regions in the DMN could be affected by RT. Moreover, the DMN includes hippocampus and other temporal regions that have been extensively reported in previous post-RT brain injury studies; therefore, DMN is an ideal functional network for us to investigate. Another potential RT-influence on the far-end regions could be the white matter structures that link to the affected near-end temporal regions. We thus use FA based on DTI to investigate the microstructural integrity of the white matter structure to further support our functional imaging-based findings.

Collectively, the hypotheses were as follows: (1) RT affects both localized functioning and functional integration in the near-end temporal lobe, particularly the hippocampus, at the acute and early response stages; (2) FC to the far-end cognitive function-related regions such as posterior cingulate cortex (PCC) in the DMN will also be affected later as some of the DMN connectivities are along the irradiation pathway; and (3) regardless of whether the brain function changes in grey matter could recover (or be plastic) or not, long-term degenerative injuries in white matter could manifest as progressively developing FA abnormalities. The innovation of our study is three-fold. First, this is the first multimodal voxel-based brain structural and functional study on the post-RT brain abnormalities using MR-normal-appearing patients with non-brain tumors. Second, this is also the first study that investigates the potential relationship between brain functional and structural changes after RT. Third, this is the first study using rs-fMRI to detect early sign of RT injury which is found to be dose dependent. Based on our results, we, for the first time, tentatively plot a recovery/progression course with respect to the post-RT brain functional and structural changes, which highlight the ability of human brain under continuous focal attacks. We also propose a preventive model that could serve as a guideline for future clinical practices to prevent or reduce the probability of RT-induced severe brain injury.

TABLE I. Demographic and clinical information of the subjects

	G1	G2	G3	G4	P
# Subjects (M/F)	25 (21/4)	24 (20/4)	19 (12/7)	19 (11/8)	0.11[a]
Age (mean±SD)	45.08 ± 8.56	44.83 ± 9.07	41.53 ± 9.63	45.00 ± 12.57	0.62[b]
T-classification	2/4/14/5	1/6/13/4	1/3/10/5	1/6/11/1	0.86[c]
N-classification	3/14/6/2	2/11/8/3	2/9/6/2	3/7/6/3	0.98[d]
M-classification	25/0	24/0	19/0	19/0	—
Tumour Overall Stage	1/5/13/6	1/5/11/7	1/3/8/7	1/6/7/5	0.98[e]
Scan Time (mo)	Pre-RT	0–6 mo	6–12 mo	> 12 mo	—
RT-injury Stage	Baseline	AC, ED	LD	LD	—
Spec Scan Time (mo)	—	3.08±1.53	10.89±1.56	33.37±19.26	—
#Subjects 2D-CRT/IMRT	—	16/8	10/9	17/2	0.05[f]
#Subjects Chemo	—	23	18	18	0.98[g]

[a]Chi-square test (*df* = 3), Chi-square = 6.035.
[b]One-way ANOVA with *F*-test, $F(3,83) = 0.60$.
[c]Chi-square test (*df* = 9), Chi-square = 4.643.
[d]Chi-square test (*df* = 9), Chi-square = 2.416.
[e]Chi-square test (df = 9), Chi-square = 2.523.
[f]Chi-square test (*df* = 2), Chi-square = 6.2.
[g]Chi-square test (*df* = 2), Chi-square = 0.04.
M: male; F: female; mo: months; scan time: the time interval in months between completion of radiotherapy and MR scan; pre-RT: prior to radiotherapy; spec scan time: the mean ± SD of specific time interval in months between completion of radiotherapy and MR scan; IMRT: intensity-modulated radiation therapy; 2D-CRT: two-dimensional conventional radiation therapy; Chemo: chemotherapy. AC: acute stage; ED: early delayed stage; LD: late-delayed stage; G1–4: groups 1–4. T-classification describes the size of the primary tumor and whether it has invaded nearby tissue and has four levels (we describe the number of patients who are, from mild to severe, T1/T2/T3/T4). N-classification describes nearby lymph nodes that are involved (four levels, N0/N1/N2/N3, from mild to severe). M-classification defines distant metastasis (no or yes, M0/M1). Tumor overall stage (I, II, III, and IV) was obtained based on the T-, N-, and M-classification results. The number of patients at each of the four stages (I/II/III/IV) is listed.

MATERIALS AND METHODS

Subjects

Newly diagnosed, treatment-naïve nasopharyngeal carcinoma patients with no brain invasion were included. Tumor stage was assessed according to the guidelines reported previously [Li et al., 2014]. The subject inclusion criteria for this study were: (1) newly diagnosed with non-keratinizing, undifferentiated nasopharyngeal carcinoma by histopathology; (2) hospitalized between 2005 and 2012; (3) no intracranial invasion; (4) clinically silent lesions; (5) neither a brain tumor nor distant metastases; (6) between 18 and 70 years of age; (7) no drinking or smoking habits; (8) no neurological or psychiatric diseases or other major medical issues; and (9) being right handed. Clinically routine MRI, including thick-slice T2- and T1-weighted images and T2 fluid-attenuated inversion recovery images, were obtained to make sure that there was no brain invasion before or any visible lesions after RT. This initial visual screening was performed by two experienced diagnostic radiologists (XL and FX, with 9 and 5 years of experience, respectively) at the initial inclusion and was verified by another diagnostic radiologist (ZD, with 24 years of experience) before data processing. Two diagnostic radiologists (XL and FX) used the internationally recommended 7th edition of the Union for International Cancer Control-American Joint Committee on Cancer (UICC-AJCC)'s Tumor, Node, Metastasis (TNM) staging system for nasopharyngeal carcinoma stage classification. The patients' TNM stage ranged from T1N0M0 to T4N2M0. All subjects underwent a detailed pretreatment evaluation, including a physical examination, nasopharyngeal fiberoptic endoscopy, MRI of the nasopharynx and neck, chest radiography, abdominal sonography, and a whole body bone scan, to exclude any associated diseases. A total of 90 patients (44.27 ± 9.79 years; range: 19–68 years; 23 females and 67 males) from Sun Yat-sen University Cancer Center were included. Based on the subsequent data processing results, three subjects were excluded due to excessive head motion. Finally, 87 subjects were included (44.22 ± 9.85 years; range: 19–68 years; 23 females). There were more males than females due to the significantly higher incidence of nasopharyngeal carcinoma in males [Chang and Adami, 2006]. There were no significant differences in age, gender, tumor TNM stage, or overall stage among the groups. For details, please see Table I. This study was approved by the Ethics Committee of Sun Yat-sen University Cancer Center. Written informed consent was obtained from the participants.

Treatments

Sixty-two of the patients in this study had been treated with RT as described earlier [Lv et al., 2014; Sun et al.,

TABLE II. Dose (in mGy) of radiation therapy for the G2 and G3 subjects

Group #	N	Dose[a] to Left Side			Dose to Right Side		
		Min	Max	Mean	Min	Max	Mean
G2	8	120.8 ± 79.4	7,150.5 ± 417.9	1,691.7 ± 469.8	108.6 ± 66.7	6,905.6 ± 587.6	1,758.1 ± 711.4
		26.8–272.1	6,211–7,583.9	813.4–2,264.1	31.1–218.8	6,213.7–7,777	817.3–3,206.8
G3	9	146.2 ± 86.2	6,831.7 ± 550.9	1,750.1 ± 616.3	132.2 ± 67	6,806.2 ± 626.2	1,695.9 ± 591.6
		29.3–283.5	5,649.9–7,639.2	1,141.9–2,863.4	27–227.8	5,475.5–7,393.9	1,069–2,717.3
G4	2	208.6–301.3	6,882.0–6,993.4	2,036.1–2,368.5	210.3–178.5	6,940.0–6,818.6	2,086.3–1,894.2
P[b]		0.54	0.20	0.83	0.48	0.74	0.85

[a]Dose refers to the dose–volume statistics applied to each side of the temporal lobe in patients who were treated with the IMRT protocol ($N = 19$, see # subjects with dose). For the dose of Groups 2 and 3, both the mean ± SD and the range are given, while for Group 4, only the range is given due to the small sample size.
[b]P: the P value generated by two-sample t test on the doses between G2 and G3. N: sample size. Left/right side: dose calculated on the left/right side of the temporal lobe; Min: the minimum dose within the RT target area in mGy; Max: the maximum dose in an area of at least 2 mm^2 within the RT target in mGy; Mean: the averaged dose in mGy across all units within the RT target area. G2: the group of subjects scanned 0–6 months after RT; G3: the group of subjects scanned 6–12 months after RT; G4: the group of subjects scanned more than 12 months after RT; RT: radiation therapy.

2013]; the remainder had not yet been treated. The RT protocol was either two-dimensional radiation therapy (2D-CRT) or intensity-modulated radiation therapy (IMRT); each patient was treated with one of them. For the 43 patients treated with 2D-CRT, the accumulated radiation dose ranged from 68 to 76 Gy, with 2 Gy per fraction applied to the primary tumor, 60 to 64 Gy applied to the involved areas of the neck, and 50 Gy applied to the uninvolved areas. For the 19 patients treated with IMRT, inverse IMRT planning was performed using the Corvus system, version 3.0 (Peacock, Nomos, Deer Park, IL), and an MIMiC multileaf collimator (Nomos, Sewickley, PA) was used for planning and treatment. The total dose with IMRT was 60–70 Gy and was divided into 30–33 fractions, with one fraction applied daily 5 days per week. Of note, 2D-CRT is a conventional technique, and IMRT, which is among the newest techniques, can reduce the probability of RT injury [Lai et al., 2011]. Because the subjects were recruited over many years, we included both 2D-CRT-treated and IMRT-treated patients. There was a significant group difference in the sample size ratio of subjects who underwent 2D-CRT and those who underwent IMRT ($P = 0.05$) that was caused by most of the subjects in G4 having been treated earlier with 2D-CRT. For the patients treated with IMRT, the dose–volume statistics for the temporal lobe were calculated [Lv et al., 2014] (Table II). Of the 62 patients who were treated, 59 with overall tumor stages II–IV received concurrent chemotherapy [Greene et al., 2002]. There was no significant group difference in the number of subjects who underwent chemotherapy.

Groups

We implemented a cross-sectional comparison strategy because the subjects were scanned only once. Based on the time between RT completion and MRI acquisition, the subjects were divided into four groups (G1, G2, G3, and G4;

$N = 25, 24, 19,$ and 19, respectively; see Table I). G1 comprised treatment-naïve nasopharyngeal carcinoma patients (i.e., pre-RT baseline), whereas G2, G3, and G4 comprised patients who had completed RT 0–6 months (including acute and early delayed stages), 6–12 months (late-delayed stage), and >12 months (late-delayed stage) before MRI acquisitions, respectively, similar to our previous study [Wang et al., 2012].

Data Acquisition

We used two noninvasive imaging modalities, rs-fMRI, and DTI. Rs-fMRI measures the blood oxygen level-dependent (BOLD) signal, which reflects spontaneous brain activity during the resting state. Rs-fMRI has the same good temporal and spatial resolution as traditional task-based fMRI, but it allows us to measure both regional brain activity and inter-regional co-activity (FC). DTI maps the diffusion of water molecules in the brain, thereby measuring the microstructural integrity of neuronal fibers in white matter. In addition, DTI-based diffusion tractography can trace major fiber bundles, the spatial substrate of the FC [Hagmann et al., 2006].

All the images were collected using a 3.0-T MR scanner (Siemens Magnetom Tim Trio, Erlangen, Germany). The imaging parameters were (1) rs-fMRI: echo-planar imaging sequence, acquisition matrix = 64×64, field of view = 230×230 mm^2, 40 axial slices, slice thickness = 3.59 mm, interslice gap = 0.73 mm, voxel size = $3.59 \times 3.59 \times 4.32$ mm^3, repetition time = 2,400 ms, echo time = 30 ms, and 240 time points (9 min 36 s); (2) high-resolution, three-dimensional T1-weighted structural MRI: magnetization prepared rapid acquisition gradient echo sequence, acquisition matrix = 256×256, field of view = 256×256 mm^2, 176 sagittal slices, no interslice gap, voxel size = $1 \times 1 \times 1$ mm^3, flip angle = 9°, echo time = 2.52 ms, inversion time = 900 ms, and repetition time = 1,900 ms; and (3) DTI:
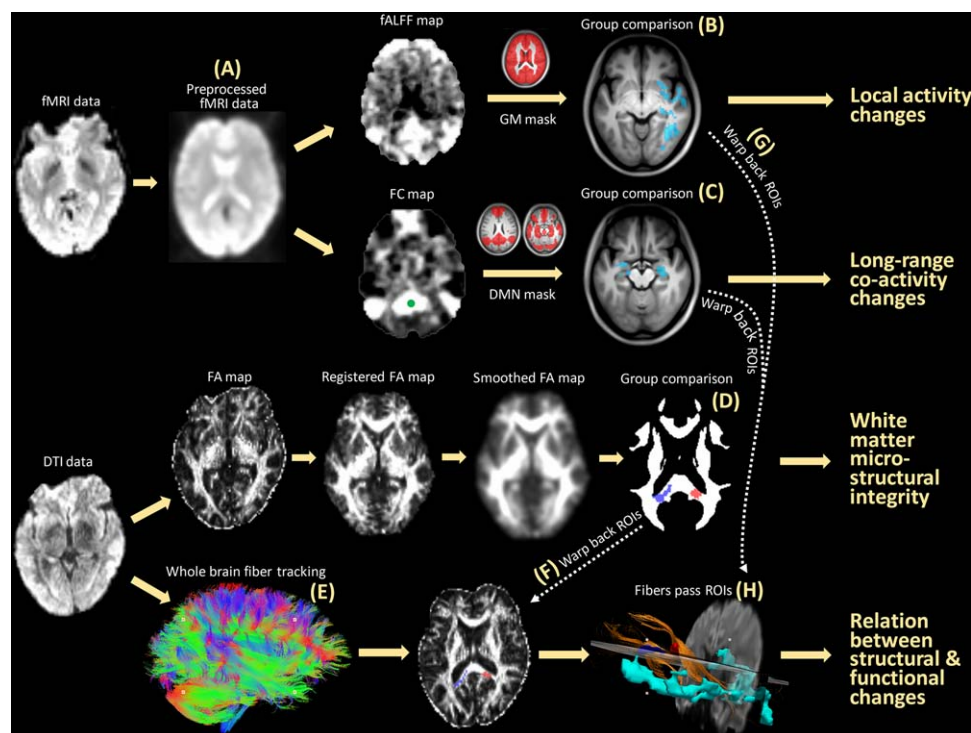
Figure 1.

Schematic flowchart of this study. With fMRI data (A), both the fALFF (measuring local activity) and the seed correlation-based FC (measuring inter-regional co-activity) were calculated and compared between G1 and the other groups (B). With DTI data, a voxel-wise comparison of the FA (measuring white matter microstructural integrity) was conducted between G1 and the other groups (D). Fiber tracking (E) was performed to link local functional changes (G) and inter-regional functional integration changes (C) with white matter changes (F, H). [Color figure can be viewed at wileyonlinelibrary.com]

echo-planar imaging sequence, acquisition matrix $= 128 \times 128$, field of view $= 256 \times 256$ mm^2, 85 axial slices, slice thickness $= 2$ mm, no interslice gap, voxel size $= 2 \times 2 \times 2$ mm^3, echo time $= 87$ ms, repetition time $= 10{,}800$ ms, one image with b $= 0$ s/mm^2, 30 images with $b = 1{,}000$ s/mm^2, and number of excitations $= 1$. The high-resolution T1 images were only used to facilitate rs-fMRI registration to the standard space. During resting state, patients were asked to not perform any explicit tasks, but to lie down, relax, and close their eyes.

Data Analysis

We used both fALFF and FC in DMN from rs-fMRI to quantify RT-induced functional abnormalities at the near-end, localized regions and the inter-regional functional connections involving far-end cognitive function-related regions. We also used FA from DTI to investigate impaired white matter and to link the near- and far-end abnormalities from a neurodegenerative viewpoint. The temporal precedence of RT-induced abnormalities in brain function and structure was investigated, along with different post-RT phases, to assess the course of post-RT

recovery and/or progression. A schematic flowchart is provided in Figure 1.

Local Activity: fALFF Analysis

The rs-fMRI and high-resolution T1 data were preprocessed with DPARSF2.2 [Yan and Zang, 2010], a toolbox based on REST1.8 [Song et al., 2011] and SPM8 (http://www.fil.ion.ucl.ac.uk/spm) in Matlab 2013a (MathWorks, Inc., Natick, MA). For rs-fMRI, the first five (12 s) images were discarded to allow for signal stabilization. The remaining data were corrected for both slice timing and head motion. Subjects with head motion >3 mm or 3° were excluded from further analyses. The T1 image was first co-registered to the rs-fMRI data and then segmented using Diffeomorphic Anatomical Registration Through Exponentiated Lie Algebra. The deformation field was then applied to the fMRI data to register them to the standard MNI space. The fMRI data were further resampled to a resolution of $3 \times 3 \times 3$ mm^3 and spatially smoothed using a 6-mm, full-width, half-maximum, isotropic Gaussian kernel. Based on the preprocessed rs-fMRI data, fALFF was calculated using the ratio of the summed BOLD

fluctuation power within the low-frequency (0.01–0.08 Hz) part of the spectrum to that within the entire frequency range [Zou et al., 2008]. Because fALFF is considered less sensitive to physiological noise and artifacts in the bottom brain, we used fALFF rather than the original amplitude of low-frequency fluctuation [Zang et al., 2007]. We first computed fALFF for every voxel in each subject, resulting in individual-level fALFF maps. These were then standardized into z-score maps by subtracting the mean voxel-wise fALFF obtained for the entire brain and dividing by the standard deviation. This standardization can improve subsequent statistical analysis and test–retest reliability [Zuo et al., 2010].

Seed-Based FC Analysis

In addition to the local activity, RT can affect FC and cause cognitive impairment. This is the first report of the use of FC in a study of post-RT brain injury. Seed-based correction, a reliable and widely adopted method in the rs-fMRI community [Shehzad et al., 2009], was used to calculate FC, which measures the synchronization of the BOLD signals from different voxels by calculating Pearson's correlation coefficients. We chose seed-based FC rather than other more complex metrics for easy interpretation [Friston, 2011]. The preprocessed rs-fMRI data were further detrended to remove linear trends due to drift, and they were band-pass filtered (0.01–0.08 Hz) to remove extremely low- and high-frequency artifacts. In addition, the averaged BOLD signal within the masks of cerebrospinal fluid and white matter and the estimated head motion parameters (Friston 24-parameter model) were regressed out to remove additional artifacts [Yan et al., 2013]. Framewise displacement (FD), the micro-head motion that has been found to influent the FC estimation, was calculated based on the method in Power et al. [2012]; the data volumes with $FD > 0.5$ were discarded, together with one data volume before and two volumes after them. After the data censoring, we further checked the remained data volumes for each subject. All the remained 87 subjects had adequate (8.96 ± 0.78 min, longer than 4.5 min) data for reliable FC calculation [Wu et al., 2015]. There was no group difference in the number of data volumes remained among the four groups (one-way ANOVA, F-test, $df = 3$, 83, $P > 0.1$). In addition, we also calculated overall translation in the three directions using mean root-mean-square (RMS) [Van Dijk et al., 2012] and overall micro-head motion using mean FD [Power et al., 2012]; there was no group difference in either metrics (one-way ANOVA, F-test, $df = 3$, 83, $P > 0.1$). To investigate FC in the DMN, a seed in the PCC [Shehzad et al., 2009] was chosen for the calculation of FC. Specifically, a 6-mm sphere centered on the PCC (MNI coordinates: -6, -58, 28) was chosen as the seed region for the FC analysis because it produces a reliable DMN. Individual FC maps were generated by calculating Pearson's correlation coefficients between BOLD signals at every brain voxel and those in the seed region. These FC maps were then transformed into z-score maps for statistical analysis by subtracting the averaged FC in the brain and dividing by the standard deviation of FC across all brain voxels.

White-Matter Microstructural Integrity: FA Analysis

FA is a scalar that describes the degree of anisotropy of a diffusion process; it has been widely used to measure the microstructural integrity (e.g., myelination) of white matter [O'Donnell and Pasternak, 2015]. A reduction in the FA is usually regarded as indicating deterioration of white-matter structural connections [Roosendaal et al., 2010; Voets et al., 2012]. Previous ROI-based FA analysis may constrain the result in specific brain regions; thus, for the first time, we calculated voxel-wise FA for the entire brain. The DTI data were processed with PANDA 1.3.0 [Cui et al., 2013], a toolbox based on FSL (http://fsl.fmrib.ox.ac.uk/fsl), Diffusion Toolkit (http://trackvis.org/dtk), and TrackVis (http://www.trackvis.org). The details of DTI data processing are summarized as follows: (1) estimating the brain mask using the $b = 0$ s/mm^2 image and the bet command of FSL to remove nonbrain regions; (2) correction for the eddy current effect by registering multiple diffusion-weighted images to the $b = 0$ s/mm^2 image with affine transformation; and (3) calculating voxel-wise diffusion tensors and FA. Note that the individual FA maps were originally calculated in native space. To allow for comparison across subjects, the FSL non-linear image registration tool, $fnirt$, was used to register each subject's FA image of native space to the FA template in the standard MNI space. The FA images of the standard space were then resampled to $2 \times 2 \times 2$ mm^3 and spatially smoothed using a 6-mm full-width half-maximum isotropic Gaussian kernel for statistical analysis.

Statistical Analysis

Statistical analyses were conducted with REST 1.8 for the rs-fMRI data and with SPM8 for the DTI data. The post-RT groups (G2, G3, and G4) were separately compared with the pre-RT group (G1) using separate two-tailed, two-sample t tests in the framework of a general linear model unless specifically indicated otherwise. Two covariates—age and gender—were added to the model during group comparisons to regress out potential nuisance effects. Different inclusive masks were used during the comparisons of different metrics according to both their biological meanings and our hypotheses. Comparisons of fALFF and FA were conducted within a gray matter mask and a white matter mask, respectively; FC was compared within a DMN mask. Specifically, for the fALFF, a whole-brain gray matter mask (applying a threshold of >0.2 to SPM8's a priori gray-matter template) was used because gray-matter voxels are generally considered to have meaningful activity. For the FC, a DMN mask was generated by conducting a one-sample t test on the

individual z-maps of the FC using all 87 subjects. A binary map was generated by applying a threshold of $P < 1 \times 10^{-12}$, which was false-discovery rate corrected ($t_{86} > 8.6$). To test if the subject's framewise head motion contributed to the group difference detected, we also included mean FD as a quantified head motion index as an additional covariate (in addition to age and gender) during the two-sample t tests, the result (not shown) was highly similar to that without head motion covariate. Therefore, framewise head motion was unlikely to affect our result of FC differences. For the voxel-wise comparison of the FA, a mask was generated by averaging the unsmoothed FA maps across all 87 subjects; the resulting FA map was binarized with a threshold of >0.4. For the FA comparisons, multiple comparison corrections were applied based on a Gaussian Random Field method in SPM8, a toolbox commonly used for voxel-based analysis of FA, with a single-tailed, voxel-level intensity threshold of $P < 0.05$ ($z > 1.65$) and an extension threshold of $P < 0.05$ (cluster size > 990 voxels). Single-tailed tests were used because of the hypothesis of reduced FA after RT. For the fALFF/FC results, a commonly used threshold for rs-fMRI studies, $P < 0.05$ after AlphaSim correction as implemented in REST was applied (i.e., two-tailed voxel-wise $P < 0.05$, randomization times $= 10{,}000$, resulting in cluster sizes >172 voxels for fALFF and >101 voxels for FC due to the different masks used in the t tests). The course of recovery/progression after RT was investigated by comparing the statistically significant changes in fALFF, FC, and FA across the three post-RT periods.

DTI Tractography

Regarding the relationship between post-RT brain functional and structural changes, we further tested whether the changes in local brain activity are related to the disrupted FC and the reduction of white matter microstructural integrity. To this end, the clusters with significant FA reduction from the analyses of DTI data were selected as the ROIs. These ROIs were transformed from the standard to the native space based on the invert warping function *invwarp* in FSL, in which the nonlinear transformation from a native FA image to the FA template was first inversed and then applied to the ROIs. Diffusion tractography was conducted to reveal the main white-matter fiber bundles that cross these ROIs using deterministic fiber tracking, as implemented by the *fact* function in FSL. Specifically, whole-brain fiber tracking was conducted first, with an automatic FA mask and an angle threshold of 40°. During fiber tracking, four seeds were randomly defined at each voxel. The main fiber bundles that intersect with each ROI were selected with TrackVis. Spatial closeness between these fibers and the gray-matter functional changes (these functional ROIs were selected based on the statistically significant results from the comparisons of fALFF and FC and warped back to the native space) was

assessed for each subject (Fig. 1). According to the hypotheses, the fiber tracts that pass the affected white-matter areas would connect to the functionally affected areas (i.e., the functional ROIs).

Follow-Ups and Retrospective Inspections

This is a prospective study consisting of the aforementioned MRI scans at the subject inclusion, and regular follow-ups for all the subjects using clinical MRI to detect MRI-visible RT-induced severe brain injury, that is, temporal lobe necrosis. Specifically, for the patients with post-RT rs-fMRI and DTI data (those in G2, G3, and G4), we conducted continuous follow-up observations every 3 months with clinical imaging sequences (T2-weighted and T2-FLAIR imaging). The patients with abnormal MR intensities in the unilateral or bilateral temporal lobe were regarded as exhibiting temporal lobe necrosis. Some patients inevitably dropped out during the follow-ups. Based on whether temporal lobe necrosis occurred during 5 years after RT completion, we retrospectively inspected the earlier brain functional/structural changes in the presymptomatic stage to search for predictive biomarkers or early signs of severe RT injury.

RESULTS

RT-Induced Local Brain Activity Changes

Compared with the baseline pre-RT group (G1), subjects in G2 (0–6 months after RT) had increased fALFF in the left inferior temporal areas (Fig. 2A) ("G2–G1" is used hereafter for comparison between G2 and G1). G2–G1 also showed an fALFF increase in the superior frontal area and an fALFF decrease in the supplementary motor area. G3–G1 showed a significant extensive decrease in the fALFF in the dispersed right temporal area and part of the supplementary motor area (Fig. 2B), but the superior frontal area still showed an fALFF increase. G4–G1 showed decreased fALFF in only a few areas in the bottom of the brain, including the bilateral hippocampus, the parahippocampus and the temporal pole, and the thalamus, brainstem, and cerebellar areas (Fig. 2C). The frontal area still had increased fALFF, which extended to the inferior frontal gyrus. In Figure 2D, the major brain regions with abnormal local activity are delineated for better illustration of the fALFF changes over time. The details of these differences are listed in Table III. We also inspected whole-brain fALFF differences with and without thresholds, and also found dynamic fALFF changes within and beyond the temporal lobe.

RT-Induced FC Changes in DMN

The seed-based correlation showed a complete DMN, consistent with previous studies; in particular, both the lateral and medial temporal cortices were included. These
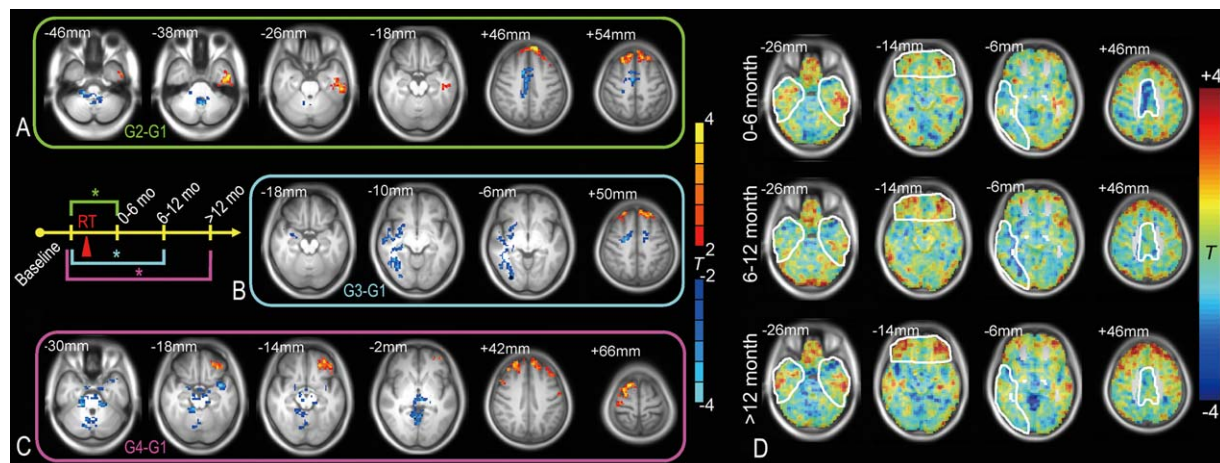
Figure 2.

Local brain activity changes after RT. Two-sample *t* tests were conducted comparing the fALFF before RT (G1, baseline group) with that at different stages after RT (G2: 0–6 months, G3: 6–12 months, G4: >12 months after completion of RT) within a grey matter mask (voxel-wise $t > 2$, AlphaSim corrected $P < 0.05$, cluster size > 172) (A–C). The result was rendered on the averaged T1 images across all subjects. The results from G2 to G1, G3 to G1, and G4 to G1 are framed with green, cyan, and purple, respectively, corresponding to the schematic plot; * indicates that a statistically significant difference was found between groups. The group comparison results are also shown without the threshold (D). The regions with abnormal local activities that changed over time are marked. The brain slices are shown in radiological convention (left is right, right is left). Details of the results are summarized in Table III. [Color figure can be viewed at wileyonlinelibrary.com]

lateral and medial temporal regions are the near-end regions exposed to the direct irradiation. The other DMN regions are thus far-end regions that could have abnormal connections to the near-end regions. There were no significant differences for G2–G1 and G4–G1. However, G3–G1 revealed a reduced FC with the PCC in various DMN regions (Fig. 3A), including the bilateral hippocampus, the parahippocampus, and other nontemporal lobe regions such as the medial prefrontal cortex, the right PCC/precuneus, and the left inferior parietal lobule (detailed in Table IV). Figure 3B shows the typical slices illustrating the FC changes within the DMN at different post-RT stages; several key regions of the DMN, including not only the hippocampus but also several frontal and parietal areas, were found to lose synchronization with the PCC. Whole-brain inspection without thresholds indicated that the above result still holds. Of note, we believed that head motion was not likely to contribute to the FC group differences because there was no group difference in either absolute or relative head motions, and because there was no visible differences in the FC different result when head motion were included as an additional covariate.

RT-Induced White-Matter Microstructural Integrity Changes

Within an FA mask in the putative white matter, there was a significant reduction in the FA value in G4–G1 (Fig. 4A) but not in G3–G1 or G2–G1. Specifically, after 12 months of the follow-ups from the completion of RT, the FA in the bilateral splenium of the corpus callosum was reduced compared to the pre-RT level (Table IV). Figure 4B clearly shows extensive FA reduction at >12 months, whereas at both 0–6 months and 6–12 months, the FA was quite stable. There was no significant post-RT late-delayed reduction in the FA within the temporal lobe white matter. The group differences in the entire white-matter mask without thresholds were also inspected and such a dynamic trend still held.

Recovery/Progression Course and "Preventive Model"

Based on the statistical analysis reported above, the course of schematic recovery/progression could be plotted (Fig. 5A). The involved regions included zones traditionally believed to be RT injury related (within the temporal lobe) and zones outside them. In the temporal lobe, the time-evolving pattern of local brain activity first increased, then decreased, and finally recovered. The most severe influence on local activity occurred in the late-delayed period (6–12 months), but there was an initial abnormal increase (<6 months). The FC with the PCC seed decreased at 6–12 months but recovered after 12 months. Functional recovery was accompanied by a gradual reduction in white-matter integrity in the corpus callosum after 12 months. Based on this temporal sequence, we derived a hypothesis for the prevention or delay of late effects,

TABLE III. Radiation-induced local brain activity changes

	Peak T value	p	Peak Z value	Cluster size	MNI coordinates	Brain region	Hemisphere
2 vs 1	−3.81	0.0004	−3.54	305	(−3, −51, −39)	Pons, Cerebellum_9	L/R
	4.43	<0.0001	4.04	352	(−45, −9, −39)	Inf/Mid/Sup_Temp, Fusiform, Hippocampus	L
	−4.19	0.0001	−3.85	508	(3, −6, 48)	Supp_Motor_Area, MCC, Paracentral_Lobule	L/R
	5.12	<0.00001	4.55	401	(21, 24, 57)	Sup/Mid_Front, Sup_Med_Front	L/R
3 vs 1	−4.79	<0.0001	−4.26	494	(33, −81, −6)	Inf/Mid/Sup_Temp, Putamen, Fusiform, Insula, Hippocampus, Parahippocampus	R
	4.34	<0.0001	3.93	270	(−21, 36, 54)	Sup/Mid_Front, Sup_Med_Front	L/R
	4.38	<0.0001	3.96	410	(9, 0, 75)	Sup/Mid_Front, Supp_Motor_Area, Precent	R
	−3.97	0.0002	−3.64	252	(21, −6, 51)	Supp_Motor_Area, MCC, Sup_Front	L/R
4 vs 1	−4.80	<0.0001	−4.27	1,646	(−42, 6, −21)	Parahippocampus, Hippocampus, Temp_Pole, Cerebelum_3/4/5/6/7b/9, Vermis_3/4/5/8, Thalamus	L/R
	5.28	<0.00001	4.61	875	(−36, 30, 48)	Sup/Mid_Front, Inf_Front_Tri/Oper, Mid_Front_Orb, Sup_Med_Front	L
	4.93	<0.0001	4.36	534	(18, 12, 66)	Sup/Mid_Front, Precent, Supp_Motor_Area	R

G2 vs G1 has a degree of freedom of 48; G3 vs G1 and G4 vs G1 have a degree of freedom of 43. The results were after $P < 0.05$, AlphaSim corrected (extension-based correction). L: left, R: right.

which we call the *preventive model*. The hypothesis under this model is that, in future, by using early brain function monitoring with fALFF, one could implement protective treatment in time that may reduce the possibility of later FC reduction and white-matter injury.

Predictive Biomarkers/Early Sign of RT Injury

To validate our proposed preventive model, we further test if the early abnormality in local fALFF could predict severe late-delayed brain injury. Based on the follow-up results, five subjects in G2 (0–6 months after RT), one subject in G3 (6–12 months after RT), and two subjects in G4 (>12 months after RT) developed temporal lobe necrosis (regarded as "bad" outcome). Those who still have normal-appearing brain imaging result after 5 years of the follow-ups were categorized as "good" outcomes. We focused on the G2 subjects because this group has relatively larger sample size with the *validated* good/bad outcomes. In the G2 group, there were five subjects with >5 years' follow-ups who still had no abnormal appearance in any part of the brain (as evaluated by clinical scans). As we have found an early abnormal increment of fALFF in this group of subjects compared with baseline pre-RT subjects in the G1 group, the averaged fALFF value within an ROI centered at the peak coordinates of G2–G1 fALFF group difference map in the temporal lobe was calculated for each subject in G1 and G2; these values were plotted in Figure 5B. As we expected, the five subjects with *bad* outcome had *greater* early fALFF increases in the left inferior temporal area than the five subjects with better outcomes. The median level of fALFF (normalized fALFF = −0.44) for the G2 subjects, as shown in Figure 5B, was able to *successfully* separate all the five subjects with bad outcomes from all the five subjects with good outcomes. Therefore, this line can be regarded as a "red line" for future RT treatment with continuous brain activity monitoring. The two subjects without later necrosis displayed fALFF values even lower than the median level of G1 subjects; these two subjects could be considered much safer.

Relationship Between Functional and Structural Changes

DTI tractography in a randomly selected subject showed a close relationship between the earlier reduction in temporal-lobe local brain activity and the later impairment of white matter integrity; this relationship was reflected by the fiber bundles connecting the two types of clusters (Fig. 6, upper panel). The fibers consist of a subset of callosal fibers that project to the temporal lobe (tapetum) and to the parietal and occipital lobes (forceps posterior); they may include the associated fibers projecting from the occipital lobe to the frontal and temporal lobes (parts of the inferior longitudinal fasciculus and the inferior fronto-
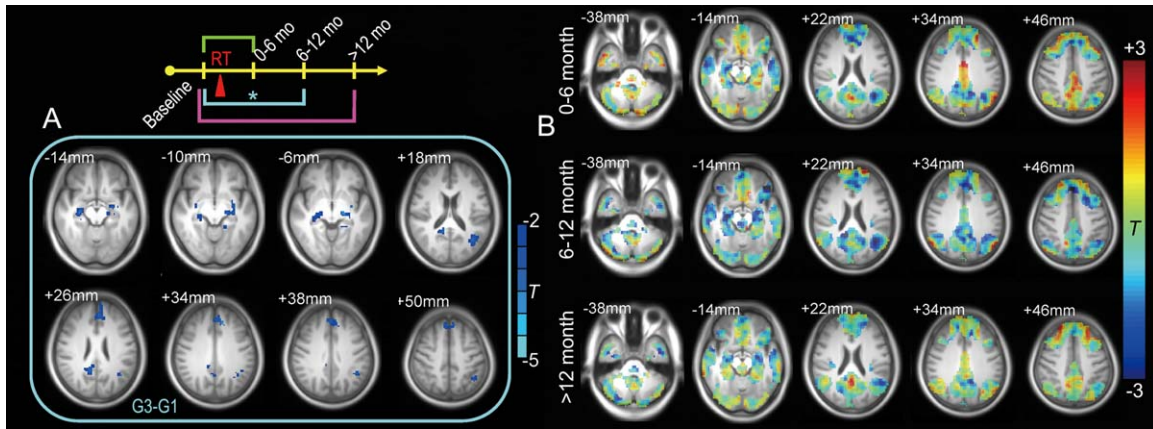
Figure 3.

RT-induced DMN functional connectivity changes. Only G3 – G1 (6–12 months after RT vs pre-RT) revealed a significant FC reduction within the DMN ($t > 2.02$, $P < 0.05$, cluster size > 101, corrected by AlphaSim) (A). The unthresholded results for each post-RT stage on typical slices of the DMN are also shown (B), with a significant whole network FC reduction at 6–12 months after RT. The results were rendered on the averaged T1 images across all subjects. The brain slices are shown in radiological convention (left is right, right is left). Details of the results are summarized in Table IV. [Color figure can be viewed at wileyon-linelibrary.com]

occipital fasciculus) [Catani and Thiebaut de Schotten, 2008]. Only fiber bundles passing through the right-sided ROI with FA difference are shown. The left-sided ROI with FA difference contained similar fiber bundles (in fact, most fibers jointly passed through the two ROIs); therefore, they are not shown. Moreover, the same fiber bundles in the same subject also connected to the ROIs with early FC reduction on both sides of the hippocampus (Fig. 6, lower panel). These interesting findings were consistent across all the subjects; that is, the fiber bundles passing through the latter FA reduction regions in the nonirradiated zone (the corpus callosum) connected the earlier far-end fALFF/FC reduction areas in the irradiated zone.

Because patients in G3 had both decreased fALFF and decreased FC in the temporal lobe 6–12 months after RT,

we performed a *post hoc* inspection and found that these results overlapped in the right hippocampus. There was a significant correlation between the fALFF and FC values in the right hippocampal ROI across all 87 subjects ($r = 0.23$, $P = 0.03$) (Fig. 7A). This means that if the fALFF in the hippocampus decreased, the FC between the PCC and the hippocampus also decreased.

Dose Dependence

Although the local brain activity seems to occur earlier in the first 6 months and be able to predict later severe consequences, we regarded this increased fALFF as a local response to irradiation. As the inter-regional FC pathway is more related to neurodegenerative process in the far-end

TABLE IV. Radiation-induced default mode network functional connectivity and white matter fractional anisotropy changes

DMN FC	Peak T value	P*	Peak Z value	Cluster size	MNI coordinates	Brain region	Hemisphere
3 vs 1	−4.17	0.0001	−3.80	169	(−18, −18, −3)	Hippocampus, parahippocampus, thalamus, amygdala	L
	−3.71	0.0006	−3.44	112	(30, −15, −15)	Hippocampus, parahippocampus	R
	−4.18	0.0001	−3.81	160	(12, −48, 24)	PCC, precuneus	L/R
	−3.57	0.0009	−3.32	222	(3, 39, 45)	Sup_Med_Front, Sup_Front, ACC	L/R
	−3.69	0.0006	−3.42	158	(−39, −57, 21)	Inf_Pariet, Mid/Sup_Temp, Angular, Supramarginal	L
DTI FA							
4 vs 1	−4.31	<0.0001	−3.91	1,256	(18, −16, 34)	Corpus Callosum_Splenium	L/R

G3 vs. G1 and G4 vs. G1 both have a degree of freedom of 43. The results were after $p < 0.05$, AlphaSim corrected for FC comparisons and were after $p < 0.05$, corrected by Gaussian random theory-based corrections, with single-tailed comparisons; L: left, R: right.
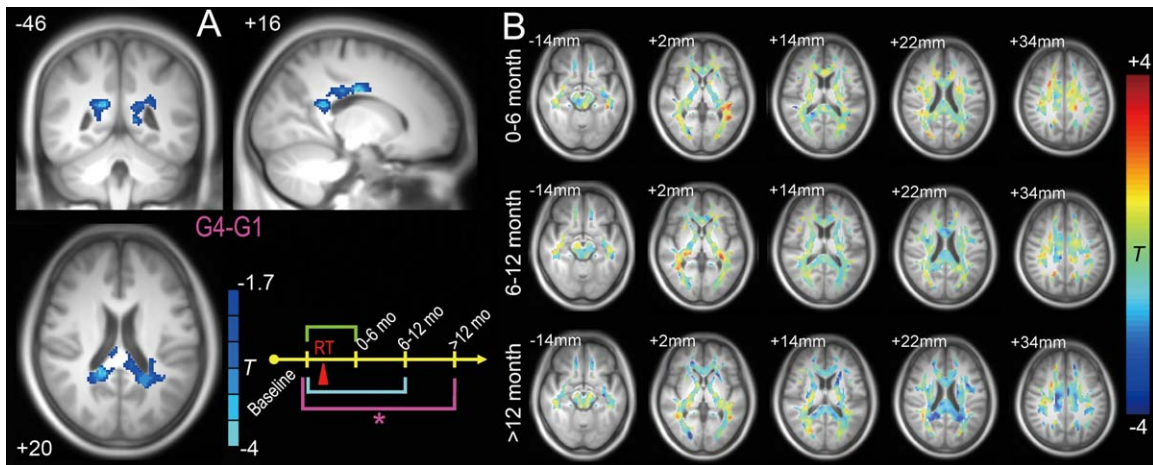
Figure 4.

FA reductions 12 months or longer from the completion of RT. Only G4– G1 reached statistical significance (Gaussian Random Field-based correction, cluster-wise $P < 0.05$, voxel-wise $P < 0.05$, single-tailed statistical test as implemented in SPM8) (A). FA changes compared with G1 (pre-RT) at all three stages are shown without thresholds in several typical slices. The underlying image is the averaged T1 image across all subjects. The brain slices are shown in radiological convention (left is right, right is left). Details are summarized in Table IV. [Color figure can be viewed at wileyonlinelibrary.com]

regions, and such a pathway could be more susceptible to RT injury due to its more exposure to irradiation, we proposed that the FC is more sensitive to irradiation dosage.

To test this hypothesis, we correlated the FC strength in the bilateral hippocampal ROIs (with FC reductions in G3–G1) with the RT doses to the temporal lobe across nine G3
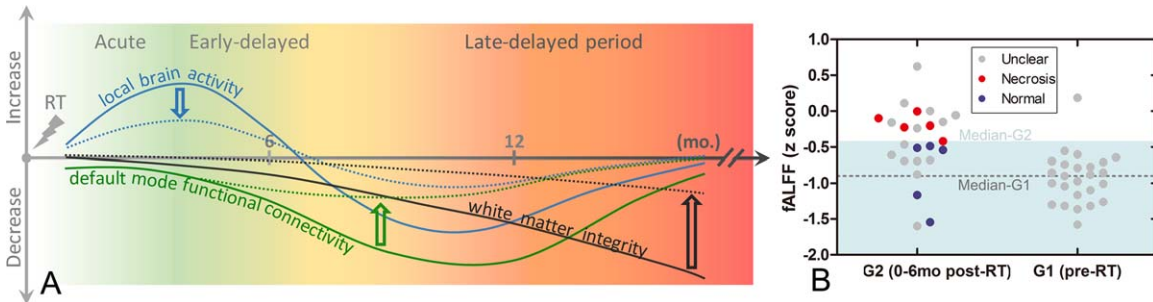

Figure 5.

Hypothesized model of different recovery/progression courses after RT with and without early intervention (A) and potential predictive biomarkers with early fALFF increments (B). In our hypothesized recovery/progressive model, a local temporal lobe brain activity increment preceded later default-mode FC and even later white matter integrity reductions. This model is plotted by the solid curves. We also proposed a preventive model, shown by the dotted curves; in this model, if the earlier local brain activity changes could be continuously monitored and carefully controlled by neuroprotective treatment, severe later white matter integrity loss and temporal lobe necrosis might be prevented. In (B), the early abnormal fALFF increment was plotted with the later outcomes (necrosis, indicating bad outcomes; or no necrosis after 5 years, indicating good outcomes) to evaluate the prognostic value of our proposed early biomarker and to further validate our preventive model. Specifically, based on the peak coordinates of G2 − G1 group differences in fALFF in the left inferior temporal lobe (-45 -9 -39, see Table III), a sphere ROI was generated (radius = 6 mm). Mean fALFF (in z score) across voxels in this ROI was extracted for each subject in G1 (pre-RT) and G2 (0–6 months after RT). Subjects showing clear temporal lobe necrosis during follow-up are shown in red; those whose brains still appeared normal are shown in blue. Subjects with unclear outcomes due to dropout are shown in gray. The median fALFF value for G2 subjects ($z = -0.44$) delineates a warning line that appears as a borderline between the light blue (safe) and the white (dangerous) zones and clearly separates the two groups of subjects with different outcomes. The median fALFF values for G1 subjects are shown by a dashed line. [Color figure can be viewed at wileyonlinelibrary.com]
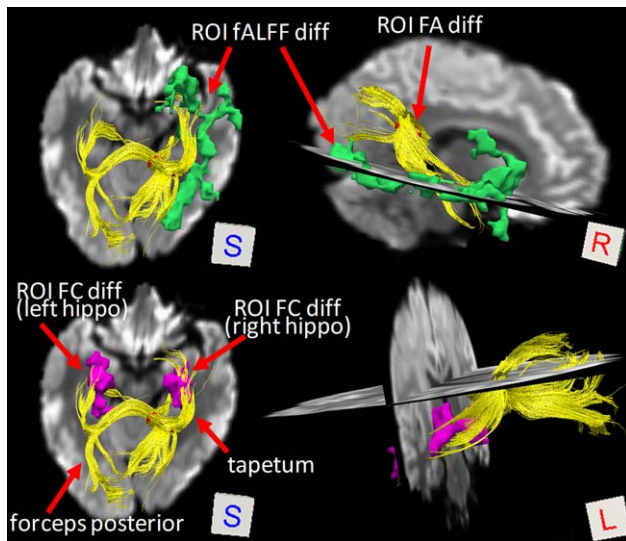
Figure 6.

Fibers connect regions showing earlier functional and later structural changes. The result shown is derived from a randomly selected subject. Fiber bundles (yellow streamlines) were found to link earlier local activity changes in the far-end temporal cortex (green clusters) and earlier default mode FC changes in the bilateral hippocampus (purple clusters) and subsequent late-delayed white-matter microstructural integrity changes in the right-side splenium of the corpus callosum (red cluster). [Color figure can be viewed at wileyonlinelibrary.com]
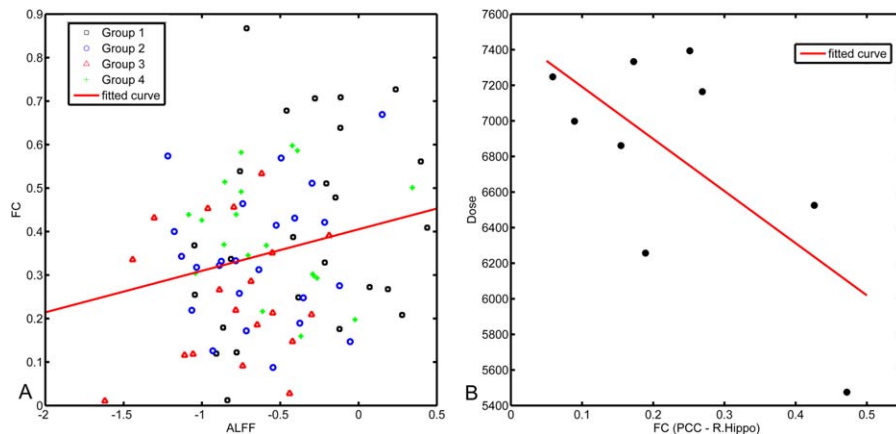
subjects receiving IMRT. There was a significant correlation between the PCC-to-right-hippocampus FC and the maximum dose applied to the right temporal lobe ($r = -0.66$, $P < 0.05$, see Fig. 7B). The higher the maximum dose, the lower the FC strength observed.

DISCUSSION

General Discussion

For the first time, we explored brain-wide RT-induced functional and structural abnormalities in normal-appearing nasopharyngeal carcinoma patients using the voxel-based analysis. We found that the brains without any visible lesions still had significant functional alterations at different post-RT stages (Figs. 2 and 3), particularly in the bilateral hippocampus. The functional changes seemed to be more sensitive than the white matter FA changes to the RT-induced injury, with the latter found to be in the splenium of the corpus callosum only after 12 months following the completion of RT, outside the zone traditionally thought to be irradiated (Fig. 4). We thus propose that the post-RT, normal-appearing brain was generally undergoing functional recovery with a structurally progressive course (Figs. 5 and 6). Interestingly, we found a dose-dependent PCC-to-right-hippocampus FC reduction in the DMN during 6–12 months after RT (Fig. 7A), indicating that the DMN FC is quite sensitive to the

Figure 7.

Correlations between the fALFF and FC values in the hippocampus (A) and between the FC and the irradiation dose (B). An intersecting ROI was generated by overlapping the fALFF reduction and FC reduction results in the G3−G1 comparison centered at the MNI coordinates of $27 - 24 - 6$ in the right hippocampus. The mean fALFF and FC values within the ROI were extracted for all subjects from all groups and plotted. The FC with the PCC and the regional fALFF correlated with one another across all subjects in all groups ($r = 0.23$, $P = 0.03$). Two ROIs in the bilateral hippocampus that showed a significantly reduced FC with the PCC in the G3−G1 comparison were selected for dose–relationship analysis. The ROIs consisted of two spheres centered at the peak MNI coordinates $30 - 15 - 15$ (right hippocampus) and $-18 - 18 -3$ (left hippocampus) with a 6 mm radius. The averaged FC on each side was correlated with the maximum and mean RT doses to the corresponding side of the temporal lobe across nine subjects who received IMRT and in whom the dose could be calculated. The maximum irradiation doses in the right temporal lobe correlated with the PCC-to-right hippocampus FC ($r = -0.66$, $P < 0.05$). [Color figure can be viewed at wileyonlinelibrary.com]

irradiation. This suggests a careful choice of the RT dose, especially the dose to the right temporal lobe, is of great importance for the prevention of late-delayed neurodegeneration. Another clinically important finding is that the early increase in fALFF can be used as a predictor of temporal lobe necrosis that may occur many years later (Fig. 5B). These findings increase our understanding of post-RT brain injury, and emphasize the need to use rs-fMRI for monitoring post-RT brain function and tailoring RT strategy.

RT-induced brain damage is not a minor issue [Greene-Schloesser and Robbins, 2012; Tsai et al., 2014]. Most patients develop cognitive and psychiatric disorders in the late-delayed period that last for years [Cheung et al., 2003; Dietrich et al., 2008; Greene-Schloesser et al., 2013; Hsiao et al., 2010; Khong et al., 2006; Mo et al., 2014; Tang et al., 2012; Warrington et al., 2013; Wu et al., 2014]. Cognitive decline can occur in patients who have no MR-visible lesions [Chapman et al., 2012; Crossen et al., 1994], a finding that suggests the presence of microscopic lesions [Atwood et al., 2007; Matulewicz et al., 2006; Nagesh et al., 2008; Warrington et al., 2013; Ye et al., 2012]. Although much progress has been made [Abayomi, 1996; New, 2001], until now no consensus has been reached for human subjects on this question [Cheung et al., 2000]. We enrolled nasopharyngeal carcinoma patients to overcome the main constraints of previous studies for better study of general RT-induced injury, especially its presymptomatic stage (MR-invisible lesions), which is most meaningful for preventive care [Chan et al., 2004]. Our results also provide guidance for tailoring the dose and identifying the region to spare during radiotherapy [Gondi et al., 2010; Kazda et al., 2014]. Importantly, two models, a functional recovery while structural progression model and a preventive model, were proposed for future RT-injury studies (Fig. 5A) and were validated by follow-ups and retrospective observations (Fig. 5B). Our result, at least from the brain structure viewpoint, confirmed that the brain structure changes could be progressive, which is consistent with previous studies which found later increased FA abnormality [Chapman et al., 2012; Nagesh et al., 2008].

This is the first-reported fMRI-based RT-injury study. Several pioneering studies using other functional modalities—for example, PET, perfusion MRI, single-photon emission computed tomography (SPECT), and MRS—have been conducted mainly to investigate RT-induced necrosis [Chan et al., 2009b; Chen et al., 2014; Chong et al., 2001; Kim et al., 2010; Matulewicz et al., 2006; Schwartz et al., 1991; Sundgren, 2009; Tsui et al., 2000, 2001] or other MR-invisible lesions [Wang et al., 2012; Xiong et al., 2013]. These results can support our findings, as fMRI is also related to cerebral vascular function and perfusion. With rs-fMRI, more detailed spatiotemporal patterns of brain function can be investigated *in vivo* [Biswal, 2012; Raichle, 2010] due to its higher spatial and temporal resolutions, which provides new information that contributes to our

understanding of RT injury obtained from the previous animal studies. Our results indicate that post-RT brain functional studies are of equal importance to white-matter structural studies because, although patients often recover from the observed functional abnormalities, these abnormalities may serve as early biomarkers of the severe temporal lobe necrosis that may develop many years later.

Early Indicators of RT Injury

One of our most important findings is the fALFF alterations in the early stage (0–6 months). Alterations at this stage have also been reported in previous studies using MRS. In a similar region, we previously found decreased N-acetylaspartic acid/choline and N-acetylaspartic acid/creatine levels at 0–6 months after RT in another nasopharyngeal carcinoma cohort [Wang et al., 2012], particularly during the first 3 months after RT [Xiong et al., 2013]. Early decreases in metabolite levels have also been reported. For example, Chen et al. [2014] found that choline/creatine decreased to its lowest level at 3 months after RT. Sundgren et al. [2009] found a decreased metabolite ratio during RT, and the reduction lasted for 6 months. However, other studies have reported different results. For example, Chan et al. [2009b] found an RT-induced increase in choline/creatine in normal-appearing mouse brain, and Matulewicz et al. [2006] found a periodic fluctuation in choline/creatine during a long post-RT period in glioma patients. The inhomogeneity of the subject cohorts, the variety of irradiation targets, and the influence of surgery and tumor recurrence could contribute to such discrepancies. In this study, these nuisance effects were largely reduced.

The increased fALFF at the inferior temporal cortex in the early stage could reflect direct disruptions of cerebral vascular function, such as disruption of the blood–brain barrier due to vascular endothelial damage [Sundgren, 2009], vascular dilation [Calvo et al., 1988; Wang et al., 2009], and increased vascularity [Schultheiss, 2012]. These changes may cause increased cerebral blood flow/volume, further causing hyperactivity. This explanation is further supported by studies involving perfusion MRI [Acker et al., 1998; Tsui et al., 2000, 2001]. In contrast, we think that neuronal dysfunction and demyelination [Chan et al., 2009b; Sundgren, 2009] are insignificant at the early stages because no decreased fALFF was found.

FALFF can be a radiosensitive early indicator. Focusing on the entire temporal lobe, we found a dynamic fALFF pattern that first increased, then decreased, and finally recovered (Fig. 2A–C). Based on the close relationship between fALFF and FC (Fig. 7A) and the common substrate between FC and white-matter integrity, we speculate that the early fALFF increase and the later fALFF/FC/FA decrease could be linked. Another important finding is that for the ten subjects in G2 whose outcome information was available, the fALFF increment in the inferior

temporal lobe at 0–6 months served as a predictive bio-marker or early sign of severe late-delayed brain injury such as temporal lobe necrosis. That is, the early fALFF alterations could be regarded as an early sign of RT injury in the presymptomatic stage many years before clear MRI-based clinical indications were present. As indicated in Figure 5B, we proposed that if a subject has significantly increased fALFF in the lower part of the temporal lobe shortly after RT, this subject may have a higher probability of developing severe RT injury after years of progression. In contrast, if a subject has stable post-RT fALFF at its pre-RT level, he/she may be much more stable and show slower progressive brain changes. In Figure 5B, we tentatively used a threshold from the median fALFF value for G2 subjects, that is, $z = -0.44$, as a warning line. For patients with fALFF above this line, neuroprotective treatments to protect brain tissue from further damage are highly recommended. Owing to the high incidence of subject dropout, only 10 subjects in G2 were used for retrospective inspections. We are currently conducting a new retrospective study with a larger sample size to further validate the predictive value of fALFF in the presymptomatic stage of RT injury. As shown in Figure 5A, we have proposed a preventive model: by monitoring brain function in the early stages with fALFF from rs-fMRI, we could reduce or prevent fALFF abnormalities in the temporal lobe by means of early intervention; later reductions in the FC and white matter integrity and even temporal lobe necrosis could be ameliorated.

Long-Term fALFF Fluctuations

In addition to the "increase-decrease-recover" pattern, we found that in specific areas of the inferior temporal lobe fALFF manifested dynamic changes with an "increase-decrease-increase" pattern (Fig. 2D, first column). This interesting fluctuation pattern is consistent with a previous report. Specifically, the interval between the two fALFF hyperintensities was approximately 6 months in our study, similar to an 8-month interval for the MRS metrics' fluctuation period [Matulewicz et al., 2006]. Our result supports the hypothesis that this fluctuation is related to the dynamic interaction between blood–brain barrier disruption and brain repair processes [Matulewicz et al., 2006]. This finding also indicates that a neuroprotective mechanism might take effect after direct injury [Chen et al., 2014], which may be one source of brain functional recovery (the other source may be the rewiring of the brain connections, see "Temporarily Disrupted and Plastic FC in the DMN").

Late-Delayed fALFF Reductions

We found a late-delayed, extensive fALFF reduction in the right temporal cortex (Fig. 2B) at 6–12 months and scattered bottom-brain fALFF reductions even after 12

months (Fig. 2C). This long-lasting reduction is supported by previous studies [Sundgren, 2009] and could be due to brain volume loss or cumulative neurotoxic effects. Interestingly, we found that the reductions occurred in the gray matter near the white matter (Fig. 2B), which further supports the hypothesis that near-end white-matter neuronal demyelination or degradation is dominant in this midterm period (in contrast to earlier gray-matter abnormalities and later far-end callosal white-matter degradation). In addition to the near-end white-matter injury, gray-matter neuronal cell death caused by apoptosis and neuronal dysfunction secondary to irradiation might also have occurred [Chan et al., 1999].

In summary, we favor a dynamic multifactorial model of RT-induced local brain function injury. That is, in earlier periods, gray matter vasculature damage dominates RT injury, whereas later demyelination (from near-end to far-end white matter, which will be discussed later) dominates the RT aftereffects. Instead of supporting either a glial hypothesis [Hopewell and van der Kogel, 1999] or a vascular hypothesis [Lyubimova and Hopewell, 2004] of white-matter damage, we believe that *both* processes exist after RT but that the two processes dominate during different stages.

An interesting lateralization in RT injury was found. For examples, late-delayed fALFF reductions occurred mainly in the right temporal lobe, and dose-dependent FC changes were also concentrated in the right hippocampus (Fig. 7B). Currently, we have no clue to the cause of this asymmetric RT influence, but previous studies have reported similar focal degenerations in the same side of the temporal lobe [Chan et al., 2009a].

The inferior and superior frontal gyri displayed increased fALFF, and this increase became more significant over time (Fig. 2). Because the frontal area is outside the irradiation field, we speculate that this was due to compensatory effects in response to temporal lobe dysfunction. Considering that all these hyperactivities are in areas related to higher cognitive functions, this compensation could help to maintain normal cognitive function. Some poststroke longitudinal studies [Levin et al., 2009] and mild cognitive impairment studies [Qi et al., 2010] have also demonstrated such compensatory effects.

Temporarily Disrupted and Plastic FC in the DMN

We found notable, distributed FC reductions in many DMN regions at 6–12 months after RT (Fig. 3). This is a significant "disruption and recovery" pattern which may indicate that the brain has the ability to recover. To our knowledge, this is a quite novel finding. This finding supports the cognitive decline, psychological disorders, and mood disorders commonly found after RT [Cheung et al., 2003; Greene-Schloesser et al., 2012; Khong et al., 2006; Mo et al., 2014; Tang et al., 2012; Wu et al., 2014] because the

DMN is essential for normal cognition and emotion [Buckner, 2013].

The decreased FC in the bilateral hippocampus is interesting. The hippocampus is an important node of the DMN [Buckner et al., 2008; Greicius et al., 2009] and is essential for learning and memory [Greicius et al., 2004]. The hippocampal cortex has dense reciprocal projections to the thalamus, midbrain, limbic system, and temporal lobe [Qin et al., 2015]. RT could impair these pathways and cause cognitive/affective disorders [Rocca et al., 2015] or directly impair the hippocampus itself [Son et al., 2015] by reducing hippocampal neurogenesis/proliferation [Conner et al., 2010; Schnegg et al., 2013] even at low radiation doses [Monje and Palmer, 2003]. Based on the dose-dependence of the FC in the hippocampus, we suggest sparing the hippocampus during RT [Gondi et al., 2010; Kazda et al., 2014] for better neurocognitive protection.

The reduction in the PCC-to-hippocampus FC is indicative of a similar phenomenon in patients with Alzheimer's disease [Greicius et al., 2004], who also suffer from mild cognitive impairment in the preclinical stage. Akiyama et al. [2001] proposed a similar hypothesis that late-delayed RT injury to the white matter occurs mainly due to demyelination, similar to clinically accelerated brain aging. The difference between the plastic FC changes observed in our study and the continuously worsening FC in Alzheimer's disease is related to the fact that our subjects had mild RT injury (MR-invisible lesions). In this cohort, the FC reduction in the late-delayed period was more flexible, possibly due to gradual cerebral vascular repair and increased numbers of neuronal cells in the affected regions [Chen et al., 2014]. Moreover, the increased FC in the frontal areas might act as a compensatory mechanism (a potential source of brain recovery following the lesions) that maintains normal cognitive function.

Far-End White-Matter Progressive Damage

Figure 4B shows clear, gradual FA reductions in the major white-matter structures, a novel and intriguing finding. DTI is a noninvasive technique that can detect white-matter damage in the absence of MR-visible lesions [Nagesh et al., 2008]. Some previous DTI studies have supported our finding of gradual white-matter damage [Nagesh et al., 2008; Welzel et al., 2008], whereas other studies have found that DTI metrics decreased in the early stage but partially recovered later [Chen et al., 2015; Wang et al., 2012; Xiong et al., 2013]. Animal studies [Chan et al., 2009b; Wang et al., 2009], however, support our finding by showing a progressive reduction in the FA with demyelination and a steeper decline when the RT dose was high. In addition, we think that the occurrence of abnormal regional functioning and inter-regional FC earlier (<12 months) than the white matter damage (>12 months) was reasonable because brain function might be more

vulnerable or sensitive to attack [Karim et al., 2016]. Interestingly, similar white-matter regions (the periventricular areas) were also found to be frequently targeted in normal aging subjects [Habes et al., 2016]. Taken together, we think our results of the white-matter progressive damage are reliable.

One possible reason for the lack of earlier stage FA reduction is that, as previously discussed, the partial volume effect and the possible registration error, particularly in the gray and white matter interface, may prevent DTI from sensitively detecting subtle changes [Schultheiss, 2012]. Therefore, our results did not indicate intact white matter in the earlier stages; rather, the white matter lesions became larger and more prominent later on [Chapman et al., 2012] and finally caused significant reductions in FA. Further studies should focus on this subtle white matter injury in the acute response stage after RT using more advanced diffusion imaging techniques with a higher spatial resolution because this earlier response could predict late injury [Chapman et al., 2012; Chen et al., 2015]. Another more likely reason for the lack of earlier stage FA reduction is that the different analytical methods used in our study (voxel-wise comparison) compared to several previous studies (ROI analysis) [Chen et al., 2015; Wang et al., 2012; Xiong et al., 2013] produced different results. In the ROI-based studies, only a small area was selected from the entire inferior longitudinal fasciculus in each subject; there is no further constraint for the ROI placement. Human intervention in the relatively subjective ROI selection has posed a serious problem. A small change in the location of the ROI may lead to large variations in FA values and biased group comparison results. Therefore, these ROI-based results may have a reliability issue. Our voxel-wised whole-brain analysis is more objective and thus more reliable.

Links Between Functional and Structural Changes

An important finding of this study is that, for the first time, we were able to link earlier RT-induced functional abnormalities with later impaired white matter integrity using DTI tractography (Fig. 6). This is also the basis of our proposed "preventive model" (Fig. 5A). Putative neuronal fiber bundles were found that connect the functional changes in the gray matter of the temporal lobe to the structural changes in the white matter outside the temporal lobe. This finding has also received support from RT-induced late response studies in which the periventricular white matter was found to undergo detectable change only after 12 months [Constine et al., 1988; Packer et al., 1986] and the large fiber bundles in the genu and splenium of the corpus callosum were found to undergo progressive structural degradation after one year [Nagesh et al., 2008], which correlated with impaired cognition [Akiyama et al., 2001]. Based on our preventive model,

protective intervention should not be exerted too late (i.e., at a time when significant FA reduction has already occurred); furthermore, the intervention should be applied *not only* to the temporal lobe *but also* to the fiber bundles that are at the far end but having dense connections to the traditionally expected irradiation damaging zone.

Clinical Implications

Our results suggest that (1) as a promising early sign, increased local brain activity in the inferior temporal lobe could be used to monitor early RT-induced brain injury at the presymptomatic stage of RT injury and to predict the occurrence of severe brain necrosis many years later; (2) the FC between the bilateral hippocampus and the PCC could be the cause of a broad spectrum of post-RT cognitive impairments as late responses; (3) whereas the FC disruption is plastic and reversible in normal-appearing brains, the potentially degenerative white-matter damage lasts longer, could be progressive, and could be a substrate of late toxicity and long-term cognitive abnormality; (4) the RT dose, particularly the maximum dose at the temporal lobe, should be carefully determined, and the course of RT should be closely monitored using fMRI; and (5) the practitioner should consider sparing the hippocampus or even the entire temporal lobe during RT.

Limitations

This study has several limitations. First, our sample size was relatively small because we used stringent subject inclusion criteria; the subjects with distant metastases were excluded to avoid any protopathic brain invasion that could interfere our results. We also only included the patients in the presymptomatic stage to explore the potential of early detection and to detect early biomarkers for developing future preventive interventions. The patients with this type of lesions are far less than those with visible lesions. In addition, we further calculated the effect size of our metrics and found that most of our results had Cohen's d values > 1 or effect size correlation r values > 0.5, indicating a large effect [Cohen, 1988; Rosnow and Rosenthal, 1996]. Second, the sample size with adequate follow-up time (until necrosis was developed or until such a possibility could be ruled out after adequately long follow-ups) is small due to uncontrollable subject dropout. Third, several patients underwent 2D-CRT, whereas other newly included patients received IMRT, and RT was combined with chemotherapy for most patients. Although these differences could be additional sources of variability [Edelmann et al., 2014], our result still shows enough effect size that indicates early brain functional changes within 6 months after RT. Fourth, only macroscopic aberrance was reported; the imaging biomarkers suggested by our results should be interpreted with more future works on the microscopic mechanisms. For example, animal studies

using both *in vivo* high-resolution rs-fMRI together with *in vitro* imaging techniques could be more specific and more helpful for unveiling the neuromechanisms of RT injury. Finally, although our study consists of follow-ups using clinical MR scans, no further rs-fMRI and DTI scans were conducted, making us impossible to track the brain changes along time within each subject. A longitudinal study is necessary to further validate our proposed models. Actually, we are carrying on a longitudinal multimodal brain imaging study on a group of newly diagnosed, treatment-naïve nasopharyngeal carcinoma patients with neither brain invasion nor MR-visible abnormalities.

CONCLUSION

Using precious multimodal brain imaging data, we revealed how the postradiotherapy brain undergoes an evolutional process with both functional recovery and structurally degenerative progression during the presymptomatic stage of RT injury. We have proposed that dynamic multifactorial processes occur in the irradiation injured presymptomatic brain involving *earlier* vasculopathology dominance and *later* demyelination dominance. Our results suggest that *both* progressive white matter degeneration from the near- to the far-end *and* neuroprotective processes and compensatory effects are involved in this recovery/progression model. Our additional preventive model highlights the importance of early brain function monitoring, careful RT-dose tailoring and timely preventive neuroprotection for avoiding irreversible severe complications that worsen outcomes.

ACKNOWLEDGMENT

REFERENCES

Abayomi OK (1996): Pathogenesis of irradiation-induced cognitive dysfunction. Acta Oncologica 35:659–663.

Acker JC, Marks LB, Spencer DP, Yang W, Avery MA, Dodge RK, Rosner GL, Dewhirst MW (1998): Serial in vivo observations of cerebral vasculature after treatment with a large single fraction of radiation. Radiation Research 149:350–359.

Akiyama K, Tanaka R, Sato M, Takeda N (2001): Cognitive dysfunction and histological findings in adult rats one year after whole brain irradiation. Neurologia medico-Chirurgica 41: 590–598.

Atwood T, Payne VS, Zhao W, Brown WR, Wheeler KT, Zhu JM, Robbins ME (2007): Quantitative magnetic resonance spectroscopy reveals a potential relationship between radiation-induced changes in rat brain metabolites and cognitive impairment. Radiation Research 168:574–581.

Biswal BB (2012): Resting state fMRI: A personal history. NeuroImage 62:938–944.

Bowen J, Gregory R, Squier M, Donaghy M (1996): The post-irradiation lower motor neuron syndrome neuronopathy or radiculopathy?. Brain: a journal of Neurology 119: 1429–1439.

Brennan B (2006): Nasopharyngeal carcinoma. Orphanet journal of rare Diseases 1:23.

Buckner RL (2013): The brain's default network: Origins and implications for the study of psychosis. Dialogues in clinical Neuroscience 15:351–358.

Buckner RL, Andrews-Hanna JR, Schacter DL (2008): The brain's default network: Anatomy, function, and relevance to disease. Annals of the New York Academy of Sciences 1124:1–38.

Calvo W, Hopewell JW, Reinhold HS, Yeung TK (1988): Time- and dose-related changes in the white matter of the rat brain after single doses of X rays. The British journal of Radiology 61:1043–1052.

Catani M, Thiebaut de Schotten M (2008): A diffusion tensor imaging tractography atlas for virtual in vivo dissections. Cortex; a journal devoted to the study of the nervous system and Behavior 44:1105–1132.

Chan AS, Cheung MC, Law SC, Chan JH (2004): Phase II study of alpha-tocopherol in improving the cognitive function of patients with temporal lobe radionecrosis. Cancer 100: 398–404.

Chan D, Anderson V, Pijnenburg Y, Whitwell J, Barnes J, Scahill R, Stevens JM, Barkhof F, Scheltens P, Rossor MN (2009a): The clinical profile of right temporal lobe atrophy. Brain: a journal of Neurology 132:1287–1298.

Chan KC, Khong PL, Cheung MM, Wang S, Cai KX, Wu EX (2009b): MRI of late microstructural and metabolic alterations in radiation-induced brain injuries. Journal of magnetic resonance imaging: JMRI 29:1013–1020.

Chan YL, Leung SF, King AD, Choi PH, Metreweli C (1999): Late radiation injury to the temporal lobes: Morphologic evaluation at MR imaging. Radiology 213:800–807.

Chan YL, Yeung DK, Leung SF, Chan PN (2003): Diffusion-weighted magnetic resonance imaging in radiation-induced cerebral necrosis. Apparent diffusion coefficient in lesion components. Journal of computer assisted Tomography 27:674–680.

Chang ET, Adami HO (2006): The enigmatic epidemiology of nasopharyngeal carcinoma. Cancer epidemiology, biomarkers & prevention: a publication of the American Association for Cancer Research, cosponsored by the American Society of Preventive Oncology 15:1765–1777.

Chapman CH, Nagesh V, Sundgren PC, Buchtel H, Chenevert TL, Junck L, Lawrence TS, Tsien CI, Cao Y (2012): Diffusion tensor imaging of normal-appearing white matter as biomarker for radiation-induced late delayed cognitive decline. International journal of radiation oncology, biology, Physics 82:2033–2040.

Chen J, Dassarath M, Yin Z, Liu H, Yang K, Wu G (2011): Radiation induced temporal lobe necrosis in patients with nasopharyngeal carcinoma: A review of new avenues in its management. Radiation Oncology 6:128.

Chen W, Qiu S, Li J, Hong L, Wang F, Xing Z, Li C (2015): Diffusion tensor imaging study on radiation-induced brain injury in nasopharyngeal carcinoma during and after radiotherapy. Tumori 101:487–490.

Chen WS, Li JJ, Zhang JH, Hong L, Xing ZB, Wang F, Li CQ (2014): Magnetic resonance spectroscopic imaging of brain injury after nasopharyngeal cancer radiation in early delayed reaction. Genetics and molecular research: GMR 13:6848–6854.

Cheung M, Chan AS, Law SC, Chan JH, Tse VK (2000): Cognitive function of patients with nasopharyngeal carcinoma with and without temporal lobe radionecrosis. Archives of Neurology 57:1347–1352.

Cheung MC, Chan AS, Law SC, Chan JH, Tse VK (2003): Impact of radionecrosis on cognitive dysfunction in patients after radiotherapy for nasopharyngeal carcinoma. Cancer 97:2019–2026.

Chong VF, Fan YF, Mukherji SK (2000): Radiation-induced temporal lobe changes: CT and MR imaging characteristics. AJR. American journal of Roentgenology 175:431–436.

Chong VF, Rumpel H, Fan YF, Mukherji SK (2001): Temporal lobe changes following radiation therapy: Imaging and proton MR spectroscopic findings. European Radiology 11:317–324.

Cohen J (1988): Statistical Power Analysis for the Behavioral Sciences. Hillsdale, NJ: Lawrence Erlbaum Associates.

Conner KR, Payne VS, Forbes ME, Robbins ME, Riddle DR (2010): Effects of the AT1 receptor antagonist L-158,809 on microglia and neurogenesis after fractionated whole-brain irradiation. Radiation Research 173:49–61.

Constine LS, Konski A, Ekholm S, McDonald S, Rubin P (1988): Adverse effects of brain irradiation correlated with MR and CT imaging. International journal of radiation oncology, biology, Physics 15:319–330.

Crossen JR, Garwood D, Glatstein E, Neuwelt EA (1994): Neurobehavioral sequelae of cranial irradiation in adults: A review of radiation-induced encephalopathy. Journal of clinical oncology: official journal of the American Society of Clinical Oncology 12:627–642.

Cui Z, Zhong S, Xu P, He Y, Gong G (2013): PANDA: A pipeline toolbox for analyzing brain diffusion images. Frontiers in human Neuroscience 7:42.

Dietrich J, Monje M, Wefel J, Meyers C (2008): Clinical patterns and biological correlates of cognitive dysfunction associated with cancer therapy. The Oncologist 13:1285–1295.

Edelmann MN, Krull KR, Liu W, Glass JO, Ji Q, Ogg RJ, Sabin ND, Srivastava DK, Robison LL, Hudson MM, Reddick WE (2014): Diffusion tensor imaging and neurocognition in survivors of childhood acute lymphoblastic leukaemia. Brain: a journal of Neurology 137:2973–2983.

Friston KJ (2011): Functional and effective connectivity: A review. Brain Connectivity 1:13–36.

Gondi V, Tome WA, Mehta MP (2010): Why avoid the hippocampus? A comprehensive review. Radiotherapy and oncology: journal of the European Society for Therapeutic Radiology and Oncology 97:370–376.

Greene-Schloesser D, Moore E, Robbins ME (2013): Molecular pathways: Radiation-induced cognitive impairment. Clinical cancer research: An official journal of the American Association for Cancer Research 19:2294–2300.

Greene-Schloesser D, Robbins ME (2012): Radiation-induced cognitive impairment–from bench to bedside. Neuro-oncology 14 Suppl 4:iv37–iv44.

Greene-Schloesser D, Robbins ME, Peiffer AM, Shaw EG, Wheeler KT, Chan MD (2012): Radiation-induced brain injury: A review. Frontiers in Oncology 2:73.

Greene FL, Balch CM, Page DL, Haller DG, Fleming ID, Morrow M, Fritz AG, editors (2002): Pharynx (Including Base of Tongue, Soft Palate and Uvula, 6th ed. New York (NY): Springer. pp 157–164.

Greicius MD, Srivastava G, Reiss AL, Menon V (2004): Default-mode network activity distinguishes Alzheimer's disease from healthy aging: Evidence from functional MRI. Proceedings of the National Academy of Sciences of the United States of America 101:4637–4642.

Greicius MD, Supekar K, Menon V, Dougherty RF (2009): Resting-state functional connectivity reflects structural connectivity in the default mode network. Cereb Cortex 19:72–78.

Habes M, Erus G, Toledo JB, Zhang T, Bryan N, Launer LJ, Rosseel Y, Janowitz D, Doshi J, Van der Auwera S, von Sarnowski B, Hegenscheid K, Hosten N, Homuth G, Volzke H, Schminke U, Hoffmann W, Grabe HJ, Davatzikos C (2016): White matter hyperintensities and imaging patterns of brain ageing in the general population. Brain: a journal of Neurology 139:1164–1179.

Haddy N, Mousannif A, Tukenova M, Guibout C, Grill J, Dhermain F, Pacquement H, Oberlin O, El-Fayech C, Rubino C, Thomas-Teinturier C, Le-Deley MC, Hawkins M, Winter D, Chavaudra J, Diallo I, de Vathaire F (2011): Relationship between the brain radiation dose for the treatment of childhood cancer and the risk of long-term cerebrovascular mortality. Brain: a journal of Neurology 134:1362–1372.

Hagmann P, Jonasson L, Maeder P, Thiran JP, Wedeen VJ, Meuli R (2006): Understanding diffusion MR imaging techniques: From scalar diffusion-weighted imaging to diffusion tensor imaging and beyond. Radiographics: a review publication of the Radiological Society of North America, Inc 26 Suppl 1: S205–S223.

Hopewell JW, van der Kogel AJ (1999): Pathophysiological mechanisms leading to the development of late radiation-induced damage to the central nervous system. Frontiers of radiation therapy and Oncology 33:265–275.

Hsiao KY, Yeh SA, Chang CC, Tsai PC, Wu JM, Gau JS (2010): Cognitive function before and after intensity-modulated radiation therapy in patients with nasopharyngeal carcinoma: A prospective study. International journal of radiation oncology, biology, Physics 77:722–726.

Jansen JF, Backes WH, Nicolay K, Kooi ME (2006): 1H MR spectroscopy of the brain: Absolute quantification of metabolites. Radiology 240:318–332.

Karim HT, Andreescu C, Tudorascu D, Smagula SF, Butters MA, Karp JF, Reynolds C, Aizenstein HJ (2016): Intrinsic functional connectivity in late-life depression: Trajectories over the course of pharmacotherapy in remitters and non-remitters. Molecular Psychiatry

Kazda T, Jancalek R, Pospisil P, Sevela O, Prochazka T, Vrzal M, Burkon P, Slavik M, Hynkova L, Slampa P, Laack NN (2014): Why and how to spare the hippocampus during brain radiotherapy: The developing role of hippocampal avoidance in cranial radiotherapy. Radiation Oncology 9:139.

Khong PL, Leung LH, Fung AS, Fong DY, Qiu D, Kwong DL, Ooi GC, McAlonan G, Cao G, Chan GC (2006): White matter anisotropy in post-treatment childhood cancer survivors: Preliminary evidence of association with neurocognitive function. Journal of clinical oncology: official journal of the American Society of Clinical Oncology 24:884–890.

Kim YH, Oh SW, Lim YJ, Park CK, Lee SH, Kang KW, Jung HW, Chang KH (2010): Differentiating radiation necrosis from tumor recurrence in high-grade gliomas: Assessing the efficacy of 18F-FDG PET, 11C-methionine PET and perfusion MRI. Clinical neurology and Neurosurgery 112:758–765.

Lai SZ, Li WF, Chen L, Luo W, Chen YY, Liu LZ, Sun Y, Lin AH, Liu MZ, Ma J (2011): How does intensity-modulated radiotherapy versus conventional two-dimensional radiotherapy influence the treatment results in nasopharyngeal carcinoma patients? International journal of radiation oncology, biology, Physics 80:661–668.

Levin MF, Kleim JA, Wolf SL (2009): What do motor "recovery" and "compensation" mean in patients following stroke?. Neurorehabilitation and neural Repair 23:313–319.

Li J, Zou X, Wu YL, Guo JC, Yun JP, Xu M, Feng QS, Chen LZ, Bei JX, Zeng YX, Chen MY (2014): A comparison between the sixth and seventh editions of the UICC/AJCC staging system for nasopharyngeal carcinoma in a Chinese cohort. PloS One 9: e116261.

Lo EH, Frankel KA, Steinberg GK, DeLaPaz RL, Fabrikant JI (1992): High-dose single-fraction brain irradiation: MRI, cerebral blood flow, electrophysiological, and histological studies. International journal of radiation oncology, biology, Physics 22: 47–55.

Lv XF, Zheng XL, Zhang WD, Liu LZ, Zhang YM, Chen MY, Li L (2014): Radiation-induced changes in normal-appearing gray matter in patients with nasopharyngeal carcinoma: A magnetic resonance imaging voxel-based morphometry study. Neuroradiology 56:423–430.

Lyubimova N, Hopewell JW (2004): Experimental evidence to support the hypothesis that damage to vascular endothelium plays the primary role in the development of late radiation-induced CNS injury. The British journal of Radiology 77: 488–492.

Matulewicz L, Sokol M, Michnik A, Wydmanski J (2006): Long-term normal-appearing brain tissue monitoring after irradiation using proton magnetic resonance spectroscopy in vivo: Statistical analysis of a large group of patients. International journal of radiation oncology, biology, Physics 66:825–832.

Mo YL, Li L, Qin L, Zhu XD, Qu S, Liang X, Wei ZJ (2014): Cognitive function, mood, and sleep quality in patients treated with intensity-modulated radiation therapy for nasopharyngeal cancer: A prospective study. Psycho-oncology 23:1185–1191.

Monje ML, Palmer T (2003): Radiation injury and neurogenesis. Current opinion in Neurology 16:129–134.

Nagesh V, Tsien CI, Chenevert TL, Ross BD, Lawrence TS, Junick L, Cao Y (2008): Radiation-induced changes in normal-appearing white matter in patients with cerebral tumors: A diffusion tensor imaging study. International journal of radiation oncology, biology, Physics 70:1002–1010.

New P (2001): Radiation injury to the nervous system. Current opinion in Neurology 14:725–734.

O'Donnell LJ, Pasternak O (2015): Does diffusion MRI tell us anything about the white matter? An overview of methods and pitfalls. Schizophrenia Research 161:133–141.

Packer RJ, Zimmerman RA, Bilaniuk LT (1986): Magnetic resonance imaging in the evaluation of treatment-related central nervous system damage. Cancer 58:635–640.

Power JD, Barnes KA, Snyder AZ, Schlaggar BL, Petersen SE (2012): Spurious but systematic correlations in functional connectivity MRI networks arise from subject motion. NeuroImage 59:2142–2154.

Qi Z, Wu X, Wang Z, Zhang N, Dong H, Yao L, Li K (2010): Impairment and compensation coexist in amnestic MCI default mode network. NeuroImage 50:48–55.

Qin S, Duan X, Supekar K, Chen H, Chen T, Menon V (2015): Large-scale intrinsic functional network organization along the long axis of the human medial temporal lobe. Brain structure & Function 221:3237–3258.

Raichle ME (2010): Two views of brain function. Trends in cognitive Sciences 14:180–190.

Rocca MA, Pravata E, Valsasina P, Radaelli M, Colombo B, Vacchi L, Gobbi C, Comi G, Falini A, Filippi M (2015): Hippocampal-

DMN disconnectivity in MS is related to WM lesions and depression. Human brain Mapping 36:5051–5063.

Roosendaal SD, Schoonheim MM, Hulst HE, Sanz-Arigita EJ, Smith SM, Geurts JJ, Barkhof F (2010): Resting state networks change in clinically isolated syndrome. Brain: a journal of Neurology 133:1612–1621.

Rosnow RL, Rosenthal R (1996): Computing contrasts, effect sizes, and counternulls on other people's published data: General procedures for research consumers. Psychol Methods 1: 331–340.

Schnegg CI, Greene-Schloesser D, Kooshki M, Payne VS, Hsu FC, Robbins ME (2013): The PPAR delta agonist GW0742 inhibits neuroinflammation, but does not restore neurogenesis or prevent early delayed hippocampal-dependent cognitive impairment after whole-brain irradiation. Free Radical Bio Med 61: 1–9.

Schultheiss TE (2012): Repair of radiation damage and radiation injury to the spinal cord. In: Jandial R, Chen M, editors. Regenerative Biology of the Spine and Spinal Cord. New York (NY): Landes Bioscience and Springer Science. pp 89–99.

Schwartz RB, Carvalho PA, Alexander E, 3rd, Loeffler JS, Folkerth R, Holman BL (1991): Radiation necrosis vs high-grade recurrent glioma: Differentiation by using dual-isotope SPECT with 201TI and 99mTc-HMPAO. AJNR. American journal of Neuroradiology 12:1187–1192.

Shehzad Z, Kelly AM, Reiss PT, Gee DG, Gotimer K, Uddin LQ, Lee SH, Margulies DS, Roy AK, Biswal BB, Petkova E, Castellanos FX, Milham MP (2009): The resting brain: Unconstrained yet reliable. Cereb Cortex 19:2209–2229.

Son Y, Yang M, Wang H, Moon C (2015): Hippocampal dysfunctions caused by cranial irradiation: A review of the experimental evidence. Brain, behavior, and Immunity 45:287–296.

Song XW, Dong ZY, Long XY, Li SF, Zuo XN, Zhu CZ, He Y, Yan CG, Zang YF (2011): REST: A toolkit for resting-state functional magnetic resonance imaging data processing. PloS One 6:e25031.

Su SF, Huang SM, Han F, Huang Y, Chen CY, Xiao WW, Sun XM, Lu TX (2013): Analysis of dosimetric factors associated with temporal lobe necrosis (TLN) in patients with nasopharyngeal carcinoma (NPC) after intensity modulated radiotherapy. Radiation Oncology 8:17.

Su SF, Huang Y, Xiao WW, Huang SM, Han F, Xie CM, Lu TX (2012): Clinical and dosimetric characteristics of temporal lobe injury following intensity modulated radiotherapy of nasopharyngeal carcinoma. Radiotherapy and oncology: journal of the European Society for Therapeutic Radiology and Oncology 104:312–316.

Sun Y, Zhou GQ, Qi ZY, Zhang L, Huang SM, Liu LZ, Li L, Lin AH, Ma J (2013): Radiation-induced temporal lobe injury after intensity modulated radiotherapy in nasopharyngeal carcinoma patients: A dose-volume-outcome analysis. BMC Cancer 13:397.

Sundgren PC (2009): MR spectroscopy in radiation injury. AJNR. American journal of Neuroradiology 30:1469–1476.

Sundgren PC, Nagesh V, Elias A, Tsien C, Junck L, Gomez Hassan DM, Lawrence TS, Chenevert TL, Rogers L, McKeever P, Cao Y (2009): Metabolic alterations: A biomarker for radiation-induced normal brain injury-an MR spectroscopy study. Journal of magnetic resonance imaging: JMRI 29:291–297.

Tang Y, Luo D, Rong X, Shi X, Peng Y (2012): Psychological disorders, cognitive dysfunction and quality of life in nasopharyngeal carcinoma patients with radiation-induced brain injury. PloS One 7:e36529.

Tang Y, Rong X, Hu W, Li G, Yang X, Yang J, Xu P, Luo J (2014): Effect of edaravone on radiation-induced brain necrosis in patients with nasopharyngeal carcinoma after radiotherapy: A randomized controlled trial. Journal of neuro-Oncology 120: 441–447.

Tsai WL, Huang TL, Liao KC, Chuang HC, Lin YT, Lee TF, Huang HY, Fang FM (2014): Impact of late toxicities on quality of life for survivors of nasopharyngeal carcinoma. BMC Cancer 14:856.

Tsui EY, Chan JH, Leung TW, Yuen MK, Cheung YK, Luk SH, Tung SY (2000): Radionecrosis of the temporal lobe: Dynamic susceptibility contrast MRI. Neuroradiology 42:149–152.

Tsui EY, Chan JH, Ramsey RG, Leung TW, Cheung YK, Luk SH, Lai KF, Wong KP, Fong D, Yuen MK (2001): Late temporal lobe necrosis in patients with nasopharyngeal carcinoma: Evaluation with combined multi-section diffusion weighted and perfusion weighted MR imaging. European journal of Radiology 39:133–138.

Van Dijk KR, Sabuncu MR, Buckner RL (2012): The influence of head motion on intrinsic functional connectivity MRI. NeuroImage 59:431–438.

Voets NL, Beckmann CF, Cole DM, Hong S, Bernasconi A, Bernasconi N (2012): Structural substrates for resting network disruption in temporal lobe epilepsy. Brain: a journal of Neurology 135:2350–2357.

Wang HZ, Qiu SJ, Lv XF, Wang YY, Liang Y, Xiong WF, Ouyang ZB (2012): Diffusion tensor imaging and 1H-MRS study on radiation-induced brain injury after nasopharyngeal carcinoma radiotherapy. Clinical Radiology 67:340–345.

Wang S, Wu EX, Qiu D, Leung LH, Lau HF, Khong PL (2009): Longitudinal diffusion tensor magnetic resonance imaging study of radiation-induced white matter damage in a rat model. Cancer Research 69:1190–1198.

Wang YX, King AD, Zhou H, Leung SF, Abrigo J, Chan YL, Hu CW, Yeung DK, Ahuja AT (2010): Evolution of radiation-induced brain injury: MR imaging-based study. Radiology 254: 210–218.

Warrington JP, Ashpole N, Csiszar A, Lee YW, Ungvari Z, Sonntag WE (2013): Whole brain radiation-induced vascular cognitive impairment: Mechanisms and implications. Journal of vascular Research 50:445–457.

Welzel T, Niethammer A, Mende U, Heiland S, Wenz F, Debus J, Krempien R (2008): Diffusion tensor imaging screening of radiation-induced changes in the white matter after prophylactic cranial irradiation of patients with small cell lung cancer: First results of a prospective study. AJNR. American journal of Neuroradiology 29:379–383.

Wong CS, Van der Kogel AJ (2004): Mechanisms of radiation injury to the central nervous system: Implications for neuroprotection. Molecular Interventions 4:273–284.

Wu X, Gu M, Zhou G, Xu X, Wu M, Huang H (2014): Cognitive and neuropsychiatric impairment in cerebral radionecrosis patients after radiotherapy of nasopharyngeal carcinoma. BMC Neurology 14:10.

Wu X, Zou Q, Hu J, Tang W, Mao Y, Gao L, Zhu J, Jin Y, Lu L, Zhang Y, Dai Z, Gao JH, Weng X, Zhou L, Northoff G, Giacino JT, He Y, Yang Y (2015): Intrinsic functional connectivity patterns predict consciousness level and recovery outcome in acquired brain injury. The Journal of neuroscience: The official journal of the Society for Neuroscience 35:12932–12946.

Xiong WF, Qiu SJ, Wang HZ, Lv XF (2013): 1H-MR spectroscopy and diffusion tensor imaging of normal-appearing temporal

white matter in patients with nasopharyngeal carcinoma after irradiation: Initial experience. Journal of magnetic resonance imaging: JMRI 37:101–108.

Yan C-G, Zang Y-F (2010): DPARSF: A MATLAB toolbox for "pipeline" data analysis of resting-state fMRI. Frontiers in systems Neuroscience 4:13.

Yan CG, Craddock RC, Zuo XN, Zang YF, Milham MP (2013): Standardizing the intrinsic brain: Towards robust measurement of inter-individual variation in 1000 functional connectomes. NeuroImage 80:246–262.

Ye J, Rong X, Xiang Y, Xing Y, Tang Y (2012): A study of radiation-induced cerebral vascular injury in nasopharyngeal carcinoma patients with radiation-induced temporal lobe necrosis. PloS One 7:e42890.

Zang YF, He Y, Zhu CZ, Cao QJ, Sui MQ, Liang M, Tian LX, Jiang TZ, Wang YF (2007): Altered baseline brain activity in children with ADHD revealed by resting-state functional MRI. Brain & Development 29:83–91.

Zeng L, Huang SM, Tian YM, Sun XM, Han F, Lu TX, Deng XW (2015): Normal tissue complication probability model for radiation-induced temporal lobe injury after intensity-modulated radiation therapy for nasopharyngeal carcinoma. Radiology 276:243–249.

Zheng Y, Han F, Xiao W, Xiang Y, Lu L, Deng X, Cui N, Zhao C (2015): Analysis of late toxicity in nasopharyngeal carcinoma patients treated with intensity modulated radiation therapy. Radiation Oncology 10:17.

Zhou GQ, Yu XL, Chen M, Guo R, Lei Y, Sun Y, Mao YP, Liu LZ, Li L, Lin AH, Ma J (2013): Radiation-induced temporal lobe injury for nasopharyngeal carcinoma: A comparison of intensity-modulated radiotherapy and conventional two-dimensional radiotherapy. PloS One 8:e67488.

Zhou X, Ou X, Xu T, Wang X, Shen C, Ding J, Hu C (2014): Effect of dosimetric factors on occurrence and volume of temporal lobe necrosis following intensity modulated radiation therapy for nasopharyngeal carcinoma: A case-control study. International journal of radiation oncology, biology, Physics 90: 261–269.

Zou QH, Zhu CZ, Yang Y, Zuo XN, Long XY, Cao QJ, Wang YF, Zang YF (2008): An improved approach to detection of amplitude of low-frequency fluctuation (ALFF) for resting-state fMRI: Fractional ALFF. Journal of neuroscience Methods 172: 137–141.

Zuo XN, Di Martino A, Kelly C, Shehzad ZE, Gee DG, Klein DF, Castellanos FX, Biswal BB, Milham MP (2010): The oscillating brain: Complex and reliable. NeuroImage 49:1432–1445.